EPMA Journal (2020) 11:661–694
https://doi.org/10.1007/s13167-020-00224-z

RESEARCH

Quantitative proteomics revealed energy metabolism pathway alterations in human epithelial ovarian carcinoma and their regulation by the antiparasite drug ivermectin: data interpretation in the context of 3P medicine

Na Li[1,2,3] · Huanni Li[4] · Ya Wang[2,3] · Lanqin Cao[4] · Xianquan Zhan[1,2,3,5,6]

Received: 18 July 2020 / Accepted: 23 September 2020 / Published online: 10 October 2020

Abstract

Objective Energy metabolism abnormality is the hallmark in epithelial ovarian carcinoma (EOC). This study aimed to investigate energy metabolism pathway alterations and their regulation by the antiparasite drug ivermectin in EOC for the discovery of energy metabolism pathway-based molecular biomarker pattern and therapeutic targets in the context of predictive, preventive, and personalized medicine (PPPM) in EOC.

Methods iTRAQ-based quantitative proteomics was used to identify mitochondrial differentially expressed proteins (mtDEPs) between human EOC and control mitochondrial samples isolated from 8 EOC and 11 control ovary tissues from gynecologic surgery of Chinese patients, respectively. Stable isotope labeling with amino acids in cell culture (SILAC)-based quantitative proteomics was used to analyze the protein expressions of energy metabolic pathways in EOC cells treated with and without ivermectin. Cell proliferation, cell cycle, apoptosis, and important molecules in energy metabolism pathway were examined before and after ivermectin treatment of different EOC cells.

Results In total, 1198 mtDEPs were identified, and various mtDEPs were related to energy metabolism changes in EOC, with an interesting result that EOC tissues had enhanced abilities in oxidative phosphorylation (OXPHOS), Kreb's cycle, and aerobic glycolysis, for ATP generation, with experiment-confirmed upregulations of UQCRH in OXPHOS; IDH2, CS, and OGDHL in Kreb's cycle; and PKM2 in glycolysis pathways. Importantly, PDHB that links glycolysis with Kreb's cycle was upregulated in EOC. SILAC-based quantitative proteomics found that the protein expression levels of energy metabolic pathways were regulated by ivermectin in EOC cells. Furthermore, ivermectin demonstrated its strong abilities to inhibit proliferation and cell cycle and promote apoptosis in EOC cells, through molecular networks to target PFKP in glycolysis; IDH2 and IDH3B in Kreb's cycle; ND2, ND5, CYTB, and UQCRH in OXPHOS; and MCT1 and MCT4 in lactate shuttle to inhibit EOC growth.

Conclusions Our findings revealed that the Warburg and reverse Warburg effects coexisted in human ovarian cancer tissues, provided the first multiomics-based molecular alteration spectrum of ovarian cancer energy metabolism pathways (aerobic glycolysis, Kreb's cycle, oxidative phosphorylation, and lactate shuttle), and demonstrated that the antiparasite drug ivermectin effectively regulated these changed molecules in energy metabolism pathways and had strong capability to inhibit cell proliferation and cell cycle progression and promote cell apoptosis in ovarian cancer cells. The observed molecular changes in energy metabolism pathways bring benefits for an in-depth understanding of the molecular mechanisms of energy metabolism heterogeneity and the discovery of effective biomarkers for individualized patient stratification and predictive/prognostic assessment and therapeutic targets/drugs for personalized therapy of ovarian cancer patients.

Keywords Epithelial ovarian carcinoma · Ivermectin · Mitochondrial proteomics · Warburg effect · Reverse Warburg effect · iTRAQ-based quantitative proteomics · SILAC-based quantitative proteomics · Energy metabolism pathway · Aerobic

Electronic supplementary material The online version of this article (https://doi.org/10.1007/s13167-020-00224-z) contains supplementary material, which is available to authorized users.

✉ Xianquan Zhan
yjzhan2011@gmail.com

Extended author information available on the last page of the article

glycolysis · Kreb's cycle · Oxidative phosphorylation · Lactate shuttle · Molecular biomarker pattern · Early diagnosis · Prognostic assessment · Predictive preventive personalized medicine (PPPM)

Introduction

Ovarian neoplasms consist of several clinic solid tumors, and their treatment depends on tumor grade and clinical stage. Epithelial ovarian carcinoma (EOC) constitutes the majority (nearly 90%) of malignant ovarian neoplasms with high mortality [1]. Despite advances in surgery, target therapy, and chemotherapy, EOC patients still have a poor 5-year overall survival rate (~ 30%) [2]. Early-stage diagnosis is a challenging clinical problem in EOC because of its hidden location [3]. Although ultrasound and cancer antigen 125 (CA-125) can be used to monitor high-risk factor women, they still cannot achieve good clinical effects [4]. The encouraging reports from the FDA in 2017 [5] show that olaparib (AZD2281), a PARP (polyADP-ribose polymerase) inhibitor, showed its efficacy on EOC patients with BRCA1 and BRCA2 mutations [6]. Therefore, it is urgently needed to develop novel molecular biomarkers for early diagnosis, treatment, and prognosis for EOC patients [7].

Proteomics was widely used in protein identification and quantification [8, 9]. Subcellular proteome research might provide more subtle clues to protein functions [10]. The mitochondria are the center of energy metabolism in eukaryotic cells; however, they are also involved in the processes of autophagy, apoptotic, cell cycle, cellular differentiation, and oxidative stress regulations [11]. All those biological processes are closely associated with tumor relapse or metastasis. Thus, exploration of mitochondria-mediated tumorigenesis and tumor progression mechanisms should be a novel way to the next generation of cancer therapeutics [12, 13]. The mitochondrial structural and morphological alterations were observed between cancer cells and control cells, and the changed structure and morphology were presumably associated with mitochondrial differentially expressed proteins (mtDEPs) [14]. Ovarian cancer mitochondrial proteomics proved that the mitochondria may mediate energy metabolism heterogeneity and chemoresistance signaling pathway [15–17]. Mitochondrial dysfunction in cancer cells is one of the important characteristics, and mitochondria-rejuvenating drugs would prevent from tumorigenesis [18]. Quantitative mitochondrial proteomics in EOC tissues revealed multiple signaling pathway changes [16, 19].

The Warburg effect and reverse Warburg effect promote the study of energy metabolic reprogramming in cancer cells [20]. The traditional Warburg effect refers to that cancer cells tend to produce ATP via glycolysis, even in aerobic condition [21]. A previous study observed increasing activity of glycolytic enzymes [22] and decreased energy production from the Kreb's cycle and oxidative phosphorylation (OXPHOS) [23]. However, in the novel "reverse Warburg effect" model, cancer cells could rely on both aerobic glycolysis and OXPHOS [24]. Oxidative stress is increased in cancer-associated fibroblasts (CAFs), and CAFs secrete plenty of nutriment to the surrounding cancer cells through aerobic glycolysis [25]. Monocarboxylate transporters (MCTs), including MCT1 and MCT4, form the "lactate shuttle" to accomplish metabolic symbiosis between cancer cells and CAFs [26]. Thus, Warburg and reverse Warburg effects are complementary to each other in the study of energy metabolic reprogramming [18]. The Warburg and reverse Warburg effects coexist in tumor tissues [27]. Upregulation and flexibility of both aerobic glycolysis and OXPHOS pathways in EOC cells have been shown previously. For example, expression of PKM2 induces a high glycolytic rate in ovarian cancer, and PKM2 inhibitor suppresses ovarian cancer cell migration and growth by disturbing Warburg effects [28]. A large number of evidence also shows contradictory findings with regard to the Warburg effect, including high mitochondrial activities and low ATP contribution of glycolysis in highly invasive ovarian cancer [29]. EOC cells presented metabolic flexibility but energy metabolic reprogramming in EOC cells remains unclear. It is necessary to study in-depth the energy metabolism inhibitors.

Ivermectin is an effective medication in the treatment of many kinds of parasites, through increasing cell membrane penetrability to cause paralysis and death of the parasites [30]. Ivermectin that was initially discovered from soil in Japan in 1973 was used in the clinic in 1981, which was collected from the list of essential medicines of the World Health Organization [31]. Satoshi Ōmura who discovered ivermectin received the Gairdner Global Health Award in 2014 and the Nobel Prize in 2015. Today, ivermectin shows multiple potential roles against bacteria and virus and as anticancer, which is continuously surprising scientists and researchers [32]. In 2004, a Russian group found that ivermectin had significant antiproliferative activity against human melanoma and a few other cancers [33]. A Chinese group reported that ivermectin regulated autophagy to suppress breast cancer growth, and found that ivermectin decreased the expression of p21-activated kinase 1 though the ubiquitination-mediated degradation pathway and resulted in the decreased phosphorylation level of Akt to block the Akt/mTOR signaling pathway [34]. Some studies also found that ivermectin induced oxidative damage and mitochondrial dysfunction in renal cell carcinoma, and ivermectin demonstrated the preferential toxicity to renal cell carcinoma rather than normal kidney cells

[35]. Ivermectin also selectively induced cell apoptosis in chronic myeloid leukemia (CML) through regulating oxidative stress and mitochondrial dysfunction [36]. However, it is still a long way for ivermectin to be applied in cancer treatment. A study found that EOC patients with worse prognosis had higher expression of oncogene KPNB1 regulating p21, p27, and APC/C family member, and ivermectin induced death of EOC cell models by inhibition of oncogene KPNB1 [37]. However, KPNB1 was not found to be a differentially expressed protein in human EOC tissues by isobaric tag for relative and absolute quantification (iTRAQ)-quantitative tissue proteomics [38] and iTRAQ quantitative tissue mitochondrial proteomics [16]. Ivermectin also blocked human epididymis protein 4/importin-4 nuclear accumulation and PAK1-dependent growth in human ovarian cancer [39, 40]. The antitumor effect of ivermectin is attracting many researches and has made some advances. However, the accurate molecular mechanism of its antitumor effect remains unclear. This study, for the first time, focused on the effects of ivermectin on energy metabolism pathways in human EOC cells through regulating energy metabolism–related enzymes to suppress EOC cell growth.

In our long-term program of EOC mitochondrial proteomics, mtDEPs were identified in EOCs compared with controls [16], and these mtDEPs were involved in multiple signaling pathways [19]. In combination with quantitative proteomics of whole EOC tissues [38], this study revealed the molecular profiling changes of energy metabolism pathways in EOC. Here is the experimental flowchart to study mtDEPs in EOCs relative to controls (Fig. 1a). Furthermore, the effect of ivermectin on human ovarian cancer cell lines was also investigated to show the roles of ivermectin in inhibiting proliferation and cell cycle progression and promoting apoptosis in EOC cells via regulating energy metabolism pathways.

Materials and methods

Ovarian cancer tissue specimen and preparation of mitochondria protein samples

Eight EOC tissues and eleven control ovaries with benign gynecologic disease (Table 1) were collected during gynecologic surgery from Chinese patients from the Department of Obstetrics and Gynecology, Xiangya Hospital, Central South University, China, after approval of Xiangya Hospital Medical Ethics Committee, and informed consent was collected from Chinese patients who had never been treated with radiotherapy or chemotherapy prior to surgery. The mitochondria were isolated and purified from EOC and control tissues with differential speed centrifugation and Nycodenz density gradient centrifugation [16, 17]. The mitochondria prepared from eight EOC tissues were combined as the EOC mitochondrial sample. The mitochondria prepared from eleven control ovaries were combined as the control mitochondrial sample. The purified mitochondria were verified with electron microscopy and western blot with different antibodies specific to different subcellular organelles, including COX4I1 (mitochondrion), flotillin-1 (cytomembrane), GM130 (Golgi apparatus), catalase (peroxisomes), cathepsin B (lysosome), and lamin B (cell nucleus). The proteins were extracted from purified mitochondrial samples for iTRAQ-labeled quantitative proteomic analysis. The detailed procedure was described previously [16, 17].

iTRAQ-based quantitative proteomics to identify mtDEPs

The extracted mitochondrial proteins (200 μg/each sample) were treated with N-hydroxysuccinimide (SDT), followed by reduction, alkylation, digestion with trypsin, and desalination. The tryptic peptides (100 μg/each sample) were labeled with iTRAQ reagents, and each sample was labeled three times. The six labeled tryptic peptide samples were equally mixed, followed by peptide fractionation with strong cation exchange (SCX) chromatography. Each SCX-fractionated sample was subject to liquid chromatography-tandem mass spectrometry (LC-MS/MS) analysis on a Q Exactive mass spectrometer (Thermo Scientific) within a 60-min LC separation gradient to obtain MS/MS data. The MS/MS data were used to identify proteins with MASCOT search engine. The iTRAQ reporter-ion intensities were used to determine each mtDEP. The mtDEP data were subject to Gene Ontology (GO) and Kyoto Encyclopedia of Genes and Genomes (KEGG) pathway enrichment analysis. The detailed procedure was described previously [16, 17].

Immunoaffinity verification of mtDEPs in tissue mitochondrial samples

One-dimensional gel electrophoresis (1DGE)-based western blot was used to verify mtDEPs (PFKP, PKM2, PDHB, CS, IDH2, IDH3A, IDH3B, OGDHL, ND2, ND5, CYTB, UQCRH, MCT1, and MCT4) between EOC and control mitochondrial samples. Because the mitochondria interact extensively with the actin cytoskeleton [41], β-actin was unavoidable to be contained in the isolated mitochondrial sample. Furthermore, iTRAQ quantitative proteomics found that β-actin (accession no. K4ENJ5) was equal between EOC and control mitochondrial samples [Ratio of T/N (T = tumor; N = control) = 1.06, $p = 0.314$] [16]. Moreover, cytochrome (Cyto), COXVI, VDAC1, and TOMM20 are commonly used as internal standard of western blot in the analysis of mitochondria; however, these proteins are all identified as differentially expressed proteins by our iTRAQ quantitative

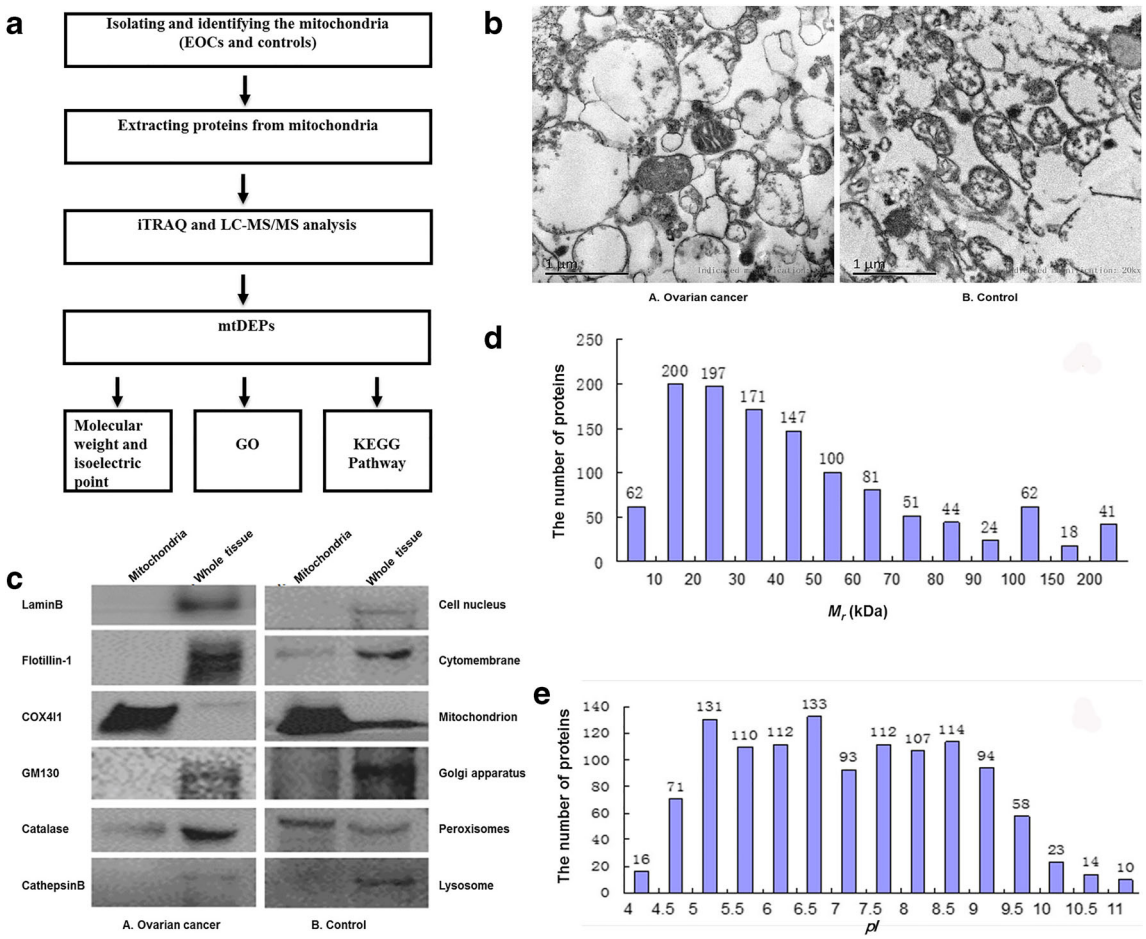

Fig. 1 Identification of mitochondrial differentially expressed proteins in EOCs relative to controls. **a** Experimental flowchart to study mitochondrial differentially expressed proteins. **b** Electron micrograph analysis of mitochondria isolated from epithelial ovarian cancer (A) and control (B) tissues. **c** Organelle-specific antibody-based western blot analysis of mitochondria isolated from epithelial ovarian cancer (A) and control (B) tissues. Equal amounts of proteins were loaded onto a 10% SDS-PAGE and analyzed by western blotting with indicated antibodies against marker proteins from the cell nucleus, cytomembrane, mitochondrion, Golgi apparatus, peroxisomes, and lysosome. **d** Distribution status of 1198 mtDEPs according to their molecular mass (M_r). **e** Distribution status of 1198 mtDEPs according to their isoelectric points (p*I*). EOC, epithelial ovarian carcinoma; SDS-PAGE, sodium dodecyl sulfate polyacrylamide gel electrophoresis; mtDEPs, mitochondrial differentially expressed proteins; iTRAQ, isobaric tags for relative and absolute quantitation; LC-MS/MS, liquid chromatography-tandem mass spectrometry; GO, Gene Ontology; GM130, golgin A2; KEGG, Kyoto Encyclopedia of Genes and Genomes; COX4I1, cytochrome *c* oxidase subunit 4I1

proteomics between ovarian cancer and control mitochondrial samples [16]. Therefore, β-actin was used as internal standard of western blot.

Ingenuity Pathway Analysis of ivermectin

Ingenuity Pathway Analysis (IPA) was used to reveal the relationship of ivermectin and potential target genes in energy metabolism pathways. IPA was the classical and very popular pathway network analysis software (http://www.ingenuity.com) [19]. Ivermectin and potential target genes in energy metabolism pathways were input into the IPA tools (build tool and grow tool) to create new "my pathway" and to show molecule networks.

SILAC-based protein quantification of effects of ivermectin on EOC cells

Stable isotope labeling with amino acids in cell culture (SILAC) labeling used kits from Thermo Fisher Scientific with RPMI 1640 lacking lysine (K) and arginine (R) supplemented with 100 mg/l [^{13}C6,^{15}N4] arginine and 100 mg/l [^{13}C6,^{15}N2] lysine with 10% dialyzed fetal bovine serum (BI-Biological Industries, Cromwell, CT, USA). TOV-21G OC cells were cultured with normal RPMI 1640 and heavy chain–labeled RPMI 1640. After 10 passages, TOV-21G cells cultured with heavy chain–labeled RPMI 1640 were treated with 20 μM ivermectin. TOV-21G cells were cultured with normal RPMI 1640 treated with DMSO. Cells were collected after 24 h of ivermectin treatment for protein extraction. The

Table 1 Clinical information of EOC and control ovary tissues that were used to prepare the mitochondria

Type of the sample	Patient no.	Age (years)	Clinical diagnosis	Pathological characteristics	Other diseases
EOC	T4	49	Stage IIIC ovarian serous cystadenocarcinoma	High-grade serous adenocarcinoma; cancer cells were found in ascites; the poorly differentiated adenocarcinoma in bilateral ovaries; metastasis of cancer cells to both sides of the fallopian tube, uterine surface, omentum majus, and intestinal wall; IHC: CK7 (+), CEA (−), CA125 (−), CDX-2 (−), WT1 (+), P63 (−), P53 (+), villin (−), CK20 (−), CK20 (−), CK19 (+), and PLAP (+−)	Moderate anemia; postoperative status of appendectomy; adenomatous polyp in transverse colon; endometrial hyperplasia; cervicitis
	T8	46	Stage IIIC poorly differentiated human ovarian adenocarcinoma	Poorly differentiated adenocarcinoma in left ovary; metastasis of cancer cells to the epiploon and peritoneum; and no metastatic carcinoma to other places	Chronic vaginitis with squamous epithelial hyperplasia; uterus leiomyoma; cervicitis; endometrial hyperplasia; hepatitis B
	T9	47	Stage IIIC ovarian serous cystadenocarcinoma	Serous cystadenocarcinoma (grades II–III and size 10 × 6.5 × 3 cm); no vascular or nerve invasiveness; metastasis of cancer cells to epiploon (size 10 × 6.5 × 3 cm); IHC: Ki67 (50%+), CA125 (+), CK (+), and CK20 (−)	Cervicitis; uterus leiomyoma; chronic salpingitis; chronic superficial gastritis
	T10	49	Stage IIIA ovarian cancer with endometrioid adenocarcinoma plus serous adenocarcinoma	Ovary mixed moderately–poorly differentiated adenocarcinoma with endometrioid adenocarcinoma plus serous adenocarcinoma; cancer embolus in right pelvic funnel ligament; no metastatic carcinoma to other places; IHC: CA125 (+), CK7 (+), CK-Pan (+), vimentin (−), ER (+) , PR (+), P53 (−), Ki67 (60%+), desmin (−), and actin (−)	Chronic cervicitis; chronic gastritis; cholecystic polypus; depressive disorder; pulmonary infection; hypoproteinemia
	T16	52	Stage IIIC moderately and poorly differentiated papillary serous adenocarcinoma in both ovaries	Moderately and poorly differentiated papillary serous adenocarcinoma in both ovaries without cancer embolus in vessel; cancer cells in right fallopian tube; no metastatic carcinoma to other places; a small amount of proliferative granulation tissue in pelvic cavity; dyskaryotic cell in ascites smear	Cervicitis with squamous hyperplasia; senile endometrium; postoperative status after resection of left breast
	T22	45	Stage IIIC moderately and poorly differentiated endometrioid adenocarcinoma in right ovary	Moderately and poorly differentiated endometrioid adenocarcinoma in right ovary (size 25 × 19 × 7 cm); no vascular or neurological invasion; metastatic carcinoma in the surface of colon sigmoideum; no metastasis to other places; IHC: Ki67 (60%+), P53 (−), ER (++), PR (+), CK7 (+), CA125 (+), CK-L (−), and CD31 (+)	Cervicitis with squamous hyperplasia; deep venous thrombosis; pleural effusion; pulmonary infection; respiratory failure type I; postoperative status after cystectomy of left ovarian cysts
	T29	45	Moderately and poorly differentiated serous ovarian carcinoma	Moderately and poorly differentiated serous ovarian carcinoma in both ovaries; no definite vascular or neurologic invasion; no metastatic carcinoma to other place; IHC: CA125 (+), ki67(30–40%+), PR (+), ER (+), villin (−), ck20 (−), CDX-2 (−), and ck7 (+)	Chronic salpingitis; chronic cervicitis
	T39	67	Stage IIC moderately and poorly differentiated mucinous papillary ovarian adenocarcinoma	Moderately and poorly differentiated mucinous papillary ovarian adenocarcinoma without cancer embolus; cancer cells in abdominal cavity; no metastatic carcinoma to other places; IHC: ki67 (30%+), wt1 (−), pax-8 (+), p%3 (+), PR (−), ER (−), and P16 (−)	Senile endometrium; chronic cervicitis with squamous metaplasia; cervical intraepithelial neoplasia (CIN grade I); hypertension; mild anemia

Table 1 (continued)

Type of the sample	Patient no.	Age (years)	Clinical diagnosis	Pathological characteristics	Other diseases
Con	C51	60	Normal ovaries	No abnormality in bilateral ovaries; mesosalpinx cyst in the right fallopian tube	Uterine prolapse (degree II); vaginal anterior wall prolapse (degree III); vaginal posterior wall prolapse (degree I); cervical intraepithelial neoplasia (CIN grade I); cervical chronic cervicitis; senile endometrium; diabetes (type II); hypertension (grade III); bronchial asthma
	C52	56	Normal ovary (right)	Ovary serous cystadenoma (left) covering with mucous epithelial cell in special mess; mesosalpinx cyst in the right fallopian tube; no abnormality in left ovary and the left fallopian tube	Ovary serous cystadenoma (left), hypertension; pelvic inflammatory disease (sequelae phase)
	C54	50	Normal ovaries	No abnormality was observed in bilateral ovaries; mesosalpinx cyst was observed in bilateral fallopian tubes	Cervical intraepithelial neoplasia (CIN grade III); chronic cervicitis with squamous epithelial hyperplasia and metaplasia; postoperative status of loop electrosurgical excision procedure (LEEP) for the treatment of CIN; HPV infection
	C55	49	Normal ovaries	No abnormality was observed in bilateral ovaries and bilateral fallopian tubes; adenomyoma and multiple leiomyoma in uterus; endometrial polyp	Cervical intraepithelial neoplasia (CIN grade III); chronic cervicitis; uterine fibroids (multiple); mild anemia; liver dysfunction
	C60	53	Normal ovaries	No abnormality was observed in bilateral ovaries and bilateral fallopian tubes	Uterine fibroids; chronic cervicitis with squamous hyperplasia; senile endometrium; fatty liver; mild anemia
	C66	44	Normal ovaries	No abnormality was observed in bilateral ovaries and left fallopian tubes; mesosalpinx cyst in right fallopian tubes; multiple uterus leiomyoma (6.5 × 7 × 9 cm, 5 × 4 × 8 cm, 5 × 3.5 × 5 cm)	Uterine fibroids; chronic cervicitis; renal hamartoma (right side)
	C68	54	Normal ovaries	No abnormality in bilateral ovaries, right fallopian tubes, vagina, and parametrial tissues; mesosalpinx cyst was observed in left fallopian tubes	Endometrial atypical hyperplasia (serious); fibrous tissue hyperplasia and glass-like changes in ligament tissues; hypertension; coronary heart disease; postoperative status after cholecystectomy
	C77	47	Normal ovary (left)	No abnormality in left ovary; cystic bleb in right ovary; effusion and cystic dilation in right fallopian tube	Ovarian follicular sac (right side); adenomyosis; chronic cervicitis with squamous metaplasia; chronic vaginitis; postoperative status after resection of left ovarian cyst
	C79	44	Normal ovary (right)	No abnormality in right ovary and bilateral fallopian tube; no cancer metastasis and enlarged lymph nodes in omentum	Ovarian serous cystadenoma (left side); postoperative status after post-hysterectomy and cystectomy of benign ovarian cysts
	C92	51	Normal ovaries	No abnormality was observed in bilateral ovaries, bilateral fallopian tubes, and parametrial tissues	Cervical intraepithelial neoplasia (CIN grade III); uterine fibroids (multiple); senile endometrium; chronic cervicitis; hypertension (grade II); hepatic cysts
	C93	52	Normal ovaries	White body formation in bilateral ovaries; multiple uterus leiomyoma (1 × 1 × 0.8 cm to 8 × 8 × 4 cm); mesosalpinx cyst in bilateral fallopian tubes	Multiple uterine fibroids; senile endometrium; chronic cervicitis; hyperlipemia

All samples were from female Chinese patients

EOC, epithelial ovarian cancer; *Con*, control ovary, *IHC*, immunohistochemistry

extracted proteins from TOV-21G cell treated with (heavy-labeling "H") and without (light-labeling "L") ivermectin were digested with trypsin, followed by peptide fractionation (n = 15 fractions), LC-MS/MS, and database searching to identify and quantify proteins in TOV-21G cells treated with (H) and without (L) ivermectin.

Effects of ivermectin on EOC biological behaviors

Two EOC cell lines (SKOV3 and TOV-21G) and one normal control cell line (IOSE80) were purchased from Keibai Academy of Science (Nanjing, China) and used in this study. First, CCK8 assay was used to detect the IC50 of ivermectin in SKOV3, TOV-21G, and IOSE80, with different concentration gradients (0–60 μM) of ivermectin for 24 h. Second, EdU assay was used to measure DNA synthesis in cells SKOV3 and TOV-21G after treatment with ivermectin (0 μM, 10 μM, 20 μM, and 30 μM) for 24 h. Third, clonogenic assay was used to investigate the in vitro effects of ivermectin in cells SKOV3 and TOV-21G after treatment with ivermectin (0 μM, 10 μM, 20 μM, and 30 μM) for 48 h. Fourth, flow cytometry was used to measure cell cycle and cell apoptosis changes in cells SKOV3 and TOV-21G after treatment with ivermectin (0 μM, 10 μM, 20 μM, and 30 μM) for 24 h.

Effects of ivermectin on target genes in energy metabolism pathways

Quantitative real-time PCR (qRT-PCR) and western blot were used to measure the mRNA and protein expressions of target genes (PFKP, PKM, CS, PDHB, IDH2, IDH3A, IDH3B, OGDHL, ND2, ND5, CYTB, UQCRH, MCT1, and MCT4) in cells SKOV3 and TOV-21G after treatment with ivermectin (0 μM, 10 μM, 20 μM, and 30 μM) 24 h treatment for RNA and 48 h for protein.

Statistical analysis

For GO and KEGG enrichment analyses and IPA analysis, p values were corrected with Benjamini–Hochberg (FDR) for multiple testing. For western blot and qRT-PCR data, data were expressed as the mean ± SD, and the statistically significant level of $p < 0.05$ was used, with Student's t test in SPSS 13.0 (SPSS Inc., Chicago, USA) (n = 3).

Results

Quality of the prepared mitochondrial samples

The mitochondrial samples from EOC and control tissues were prepared with differential speed centrifugation and Nycodenz density gradient centrifugation [16, 17], followed by quality evaluation with electron microscopy and western blot. Electron microscopic images showed that mitochondria were present as main organelles in the prepared EOC and control mitochondrial samples (Fig. 1b). No other organelles and cell debris were found except a small amount of peroxisomes, which demonstrated that the quality of the prepared mitochondrial samples was very good. Moreover, the quality of mitochondrial samples was also evaluated by western blotting with the antibodies of subcellular organelles' feature proteins such as COX4I1, flotillin-1, GM130, catalase, cathepsin B, and lamin B (Fig. 1c). COX4I1 was specifically located in mitochondrion, flotillin-1 in cytomembrane, GM130 in Golgi apparatus, catalase in peroxisome, cathepsin B in lysosome, and lamin B in cell nucleus. For the whole tissue samples, all subcellular organelles were detected in EOC and control tissues. For the prepared mitochondrial samples, only mitochondria were detected as the major component in EOCs and controls, respectively (Fig. 1c), whereas the cell nucleus, Golgi apparatus, and lysosome were not detected at all. A certain amount of peroxisomes and cytomembranes were detected (Fig. 1c), which is very reasonable because mitochondria interact extensively with the cytosol cytoskeleton [41] and peroxisomes [42] to further reflect the functional complexity of mitochondria. These results clearly demonstrated that the prepared mitochondrial samples were of a very good quality.

The mtDEP profiling in EOC

In total, 1198 mtDEPs between EOC and control mitochondrial samples were determined with iTRAQ-SCX-LC-MS/MS (Supplementary Table 1) [17]. Those mtDEPs were mostly distributed within a M_r range of 10–200 kDa (Fig. 1d) and a pI range of 4–11 (Fig. 1e). No protein was detected in the area of pI < 4 and the majority of proteins were within pI 4–10, which showed good consistency of pI distribution pattern in this study compared with that of a previous study [43]. Moreover, most of mtDEPs were localized within the mitochondria. However, some DEPs were not annotated in the mitochondria but in other cellular compartments, and the reason for this observation would be that these DEPs were derived from the proteins that interacted with outer mitochondrial membrane or mitochondria-related proteins [44].

Furthermore, functional analysis revealed that those 1198 mtDEPs were involved in multiple biological processes. Especially interesting was the observation that mitochondrial ribosome and energy metabolism pathways were significantly changed. iTRAQ quantitative proteomics found 17 mitochondrial ribosome proteins were changed, including MRPL41, MRPL46, MRPL49, MRPL51, MRPL52, MRPL53, MRPL54, MRPL55, MRPS10,

Table 2 DEPs in ribosome-associated proteins

Accession no.	Protein	Unique peptides	Coverage (%)	PSMs	calc. p*I*	MW (kDa)	Ratio (T/N)	*p* value (*t* test)
O15235	28S ribosomal protein S12, mitochondrial	1	5.8	1	10.3	15.2	2.3	1.21E-03
P82914	28S ribosomal protein S15, mitochondrial	10	33.07	20	10.5	29.8	1.5	7.14E-03
E9PE17	28S ribosomal protein S17, mitochondrial (fragment)	4	51.94	10	9.8	14.4	1.8	1.52E-03
A0A075B746	28S ribosomal protein S21, mitochondrial	3	39.08	6	9.9	10.7	2.0	3.18E-03
Q9Y3D9	28S ribosomal protein S23, mitochondrial	7	40.53	24	8.9	21.8	1.8	1.06E-03
C9JBY7	28S ribosomal protein S33, mitochondrial	2	21.88	3	10.2	11.4	1.5	6.00E-03
P82932	28S ribosomal protein S6, mitochondrial	5	39.2	11	9.3	14.2	2.6	1.33E-03
P82933	28S ribosomal protein S9, mitochondrial	13	39.14	29	9.5	45.8	1.6	1.98E-02
Q8IXM3	39S ribosomal protein L41, mitochondrial	5	38.69	9	9.6	15.4	1.5	3.78E-02
Q9H2W6	39S ribosomal protein L46, mitochondrial	8	36.92	13	7.0	31.7	1.5	7.89E-03
Q13405	39S ribosomal protein L49, mitochondrial	5	30.12	6	9.5	19.2	1.6	2.91E-03
Q4U2R6	39S ribosomal protein L51, mitochondrial	1	5.47	1	11.3	15.1	1.6	8.25E-03
G5E9P5	39S ribosomal protein L52, mitochondrial	1	30	1	9.5	11.7	1.8	2.20E-02
Q96EL3	39S ribosomal protein L53, mitochondrial	4	43.75	9	8.8	12.1	1.6	5.88E-04
Q6P161	39S ribosomal protein L54, mitochondrial	3	48.55	6	9.6	15.8	1.8	8.11E-03
X6RIW1	39S ribosomal protein L55, mitochondrial (fragment)	1	10.53	2	11.9	8.6	1.6	9.50E-03
P05141	ADP/ATP translocase 2	6	49.66	304	9.7	32.8	1.8	1.21E-03
Q6PI41	AURKAIP1 protein (fragment)	1	6.17	3	10.5	18.6	2.0	8.96E-04
B4DP77	cDNA FLJ57413, highly similar to Mitochondrial 28S ribosomal protein S10	4	35	11	6.4	18.7	1.6	1.12E-02
Q96RP9	Elongation factor G, mitochondrial	25	36.22	56	7.0	83.4	1.9	9.21E-04
P43897	Elongation factor Ts, mitochondrial	12	43.69	32	8.4	35.4	1.6	2.12E-03
P49411	Elongation factor Tu, mitochondrial	29	63.27	251	7.6	49.5	1.5	2.10E-03
Q96DP5	Methionyl-tRNA formyltransferase, mitochondrial	2	5.4	2	9.7	43.8	1.5	1.15E-04
Q9UBX3	Mitochondrial dicarboxylate carrier	1	34.49	12	9.5	31.3	2.5	1.06E-02
Q8TEM1	Nuclear pore membrane glycoprotein 210	19	13.14	30	6.8	205.0	1.5	1.39E-02
Q9Y5M8	Signal recognition particle receptor subunit beta	11	44.28	37	9.0	29.7	1.5	1.88E-02
Q9BSK2	Solute carrier family 25 member 33	1	6.85	3	9.6	35.4	1.6	1.40E-02

T/N refers to protein ratio of EOC/control

DEP, differentially expressed protein; *MW*, molecular weight; *pI*, isoelectric point; *PSMs*, peptide spectrum matches

MRPS12, MRPS15, MRPS17, MRPS21, MRPS23, MRPS33, MRPS6, and MRPS9, which were all upregulated (Table 2). Mitochondrial ribosome was a protein complex that monitors mitochondrial translation for mRNAs encoded in mtDNA. It revealed that mitochondrial functions and its involved pathophysiological activities were unavoidably changed. A quantitative analysis of mitochondrial ribosome proteins can reveal mechanisms of mitochondrial translational control. Though most of the mitochondrial proteins are synthesized by cytoplasmic ribosomes, the crucial protein components in the electron transport chain (ETC) complexes are partially translated in the mitochondria [45]. It clearly demonstrated that the mitochondrial ribosome function was changed in EOC, which results in changes of its synthesized key protein components in the ETC complex to affect energy metabolism in EOC.

Enhanced activities of three energy metabolism pathways in EOCs

A previous iTRAQ-labeled quantitative proteomic study between EOC and control whole tissues found that the key enzymes in the glycolysis pathway [38], located in the cytoplasm, were significantly upregulated in the EOC relative to control tissues. It demonstrated the increased activities of glycolysis pathway in EOC tissues, which coincided with the Warburg effect proposed in 1926 [46]. Moreover, the KEGG pathway analysis of those 1198 mtDEPs found that the Kreb's cycle and OXPHOS pathways, located in the mitochondria, were significantly involved in the identified mtDEPs, and the key proteins (PDHB, CS, IDH2, OGDHL, and UQCRH) in the OXPHOS and Kreb's cycle pathways were significantly upregulated. It demonstrated the increased

activities of OXPHOS and Kreb's cycle pathways in EOC tissues, namely the reverse Warburg effect [24].

(i) The enhanced glycolysis: iTRAQ-SCX-LC-MS/MS analysis of the whole tissue samples revealed that the glycolysis-related enzymes were significantly increased in EOC tissues relative to controls, including phosphofructokinase platelet (PFKP), pyruvate kinase muscle (PKM), lactate dehydrogenase B (LDHB), lactate dehydrogenase A (LDHA), enolase 1 (ENO1), alcohol dehydrogenase 5 class III chi polypeptide (ADH5), and glucose-6-phosphate isomerase (GPI) (Fig. 2 and Table 3) [38]. Among them, PFKP (fold change = 1.90, p = 2.28E-2) and PKM (fold change = 2.38, p = 1.50E-4) were the rate-limiting enzymes. PFKM took part in an irreversible reaction in the process of glycolysis, and it served as one of the rate-limiting enzymes. Pyruvate kinase catalyzed the final step of glycolysis to form pyruvate and ATP. GPI (fold change = 1.31, p = 2.96E-2) was not the rate-limiting enzyme of glycolysis but was one of the important regulatory enzymes. GPI protein has different functions inside and outside the cell; it was involved in the breakdown and buildup of glucose in the cytoplasm inside the cell or acted as neuroleukin outside the cell [47]. In short, those results demonstrated that EOC relied mainly on high levels of glycolysis.

(ii) The enhanced Kreb's cycle: Quantitative mitochondrial proteomics revealed that the related enzymes of Kreb's cycle were significantly increased in EOCs relative to controls, including CS, IDH, OGDHL, SUCLG2, FH, MDH2, and PDHB (Fig. 3 and Table 4). Among them, CS (fold change = 1.59, p = 4.00E-3), IDH2 (fold change = 2.02, p = 2.00E-3), IDH3A (fold change = 0.56, p = 2.54E-3), IDH3B (fold change = 1.60, p = 2.20E-2), and OGDHL (fold change = 1.55, p = 1.00E-3) were the rate-limiting enzymes. It is well-known that the enzyme pyruvate dehydrogenase complex (PDC) converted pyruvate to acetyl CoA by pyruvate decarboxylation, which connected cytoplasmic glycolysis with mitochondrial Kreb's cycle. What was notable in the PDC was that PDHB (fold change = 1.75, p = 0.008) as one subunit of PDC was obviously upregulated in EOC tissues. Those findings demonstrated that EOC had an enhanced Kreb's cycle, which coincided with the well-known reverse Warburg effect.

(iii) The enhanced OXPHOS: In most eukaryotes, Kreb's cycle-generated NADH and FADH2 were fed into OXPHOS inside the mitochondria. The eukaryotic ETCs contain complex I—NADH-coenzyme Q oxidoreductase, complex II—succinate-Q oxidoreductase, complex III—Q-cytochrome *c* oxidoreductase, complex IV—cytochrome coxidase, and complex V—ATP synthase. The expressions of complex III subunits (CYTB and UQCRH), complex IV (COX17, COX4I2, COX6C, COX7A2L, COX7A2, COX1, and COX2), and complex V (ATP6, ATP5G1, ATP6V0C, and ATP6V1D) were significantly upregulated in EOC tissues (Fig. 4 and Table 5). It clearly demonstrated that the eukaryotic ETCs were enhanced in EOC tissues. The main function of the mitochondria was to produce ATP and ROS [48]. Although the implications of electron "leakage" was not always clear, ROS productions were increased in cancer cells compared with normal cells [49]. Thus, the increase of ROS productions in cancer cells enhanced oxidative stress in stromal CAFs, which coincided with the well-known reverse Warburg effect.

Western blot validation of the rate-limiting enzymes in energy metabolism pathways

For validation of mtDEPs identified with iTRAQ-SCX-LC-MS/MS, those rate-limiting enzymes were further analyzed with western blot, including PKM2, PDHB, CS, IDH2, OGDHL, and UQCRH, between human EOC and control mitochondrial samples. Western blot found that the protein levels of PDHB, CS, IDH2, OGDHL, and UQCRH were significantly increased in EOCs relative to controls (Fig. 5 a and b), whereas PKM2 showed a rising trend without a statistical significance. The western blot results showed a very good consistency with the results of iTRAQ quantification and also confirmed the enhanced capabilities of three energy metabolism pathways (Kreb's cycle, OXPHOS, and glycolysis) in EOC tissues.

The Warburg and reverse Warburg effects in EOCs

Some cancer cells mainly depended on aerobic glycolysis, whereas other cancer cells depended mainly on OXPHOS for energy supply. The evidence proved that "Warburg effect" and "reverse Warburg effect" coexisted in a population of cancer cells such as a cancer tissue. Cancer cells released ROS into extracellular interstitium, which resulted in CAFs in a state of stress and produced lots of nourishment for ATP generation through Kreb's cycle and OXPHOS (Fig. 5c). Our previous study [17] found that MCT1 and MCT4, which link the oxidative cancer cells and the high glycolytic cancer cells/CAFs, were significantly upregulated in EOC cells (SKOV3 and TOV21G) compared with ISOE80 normal cells by qRT-PCR analysis, with the fold change of MCT-1 in SKOV3 cells (fold change = 3.70, p = 0.009) and in TOV21G cells (fold change = 2.67, p = 0.005) and with the fold change of MCT-4 in SKOV3 cells (fold change = 5.93, p

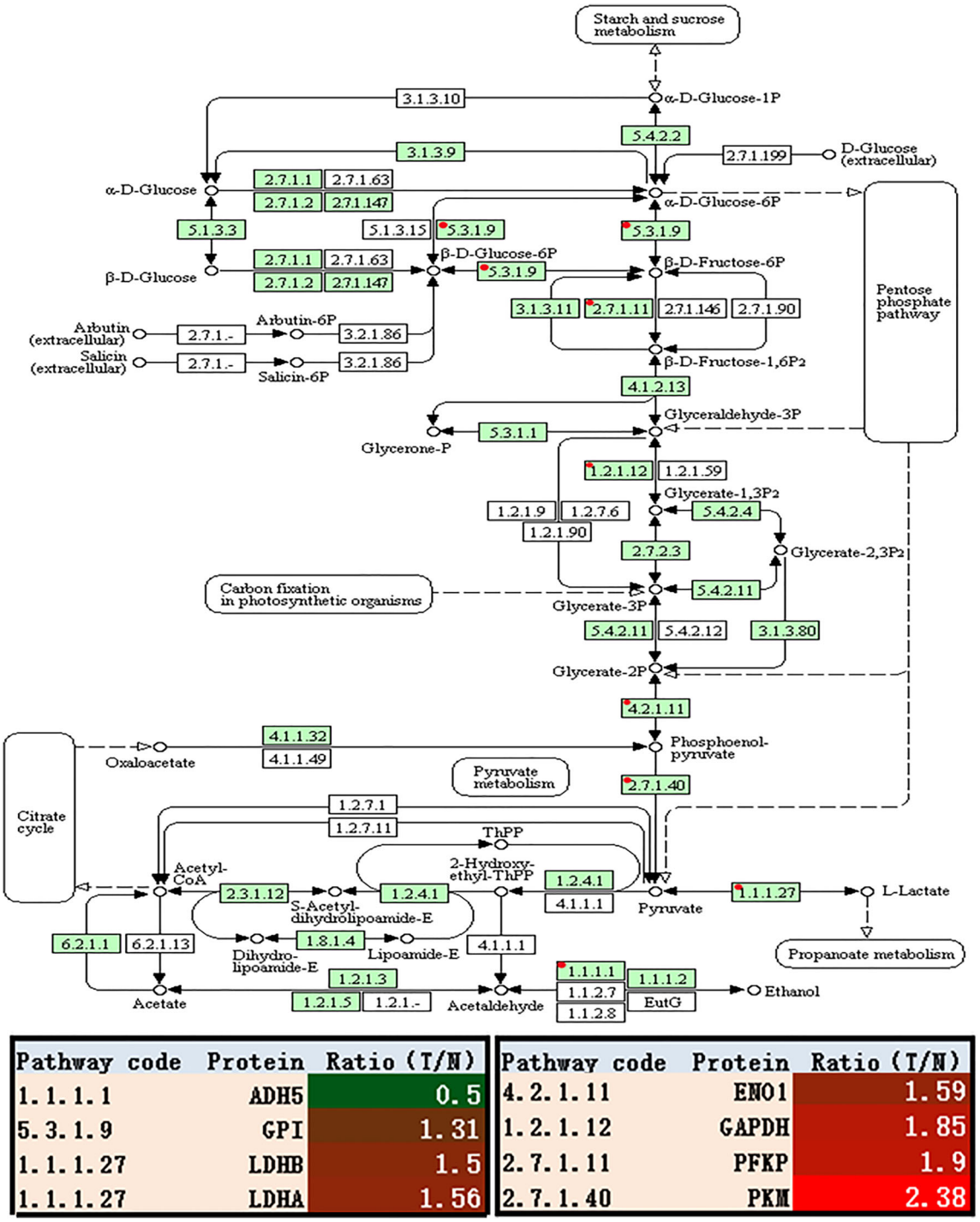

Pathway code	Protein	Ratio (T/N)
1.1.1.1	ADH5	0.5
5.3.1.9	GPI	1.31
1.1.1.27	LDHB	1.5
1.1.1.27	LDHA	1.56

Pathway code	Protein	Ratio (T/N)
4.2.1.11	ENO1	1.59
1.2.1.12	GAPDH	1.85
2.7.1.11	PFKP	1.9
2.7.1.40	PKM	2.38

Fig. 2 Glycolysis/gluconeogenesis pathway altered in epithelial ovarian cancer. Green rectangle with red mark means the differentially expressed proteins. Green rectangle without red mark means species-specific enzymes. White rectangle means reference pathway. The solid line means molecular interaction. The dot line means indirect effect. The circle means mostly chemical complex. ADH5, alcohol dehydrogenase 5 class III chi polypeptide; GPI, glucose-6-phosphate isomerase; LDHB, lactate dehydrogenase B; LDHA, lactate dehydrogenase A; ENO1, enolase 1; GAPDH, glyceraldehyde-3-phosphate dehydrogenase; PFKP, phosphofructokinase, platelet; PKM, pyruvate kinase muscle

= 0.002) and in TOV21G cells (fold change = 10.38, p = 0.00001). The western blot results showed a very good consistency with the results of qPCR quantification and also confirmed significantly increased levels of MCT1 and MCT4 in EOCs (both tissue and cell samples) relative to controls (Fig. 5d).

Table 3 Glycolysis pathways involved DEPs operated in ovarian cancer biological system

Pathway code	Accession no.	Protein	calc. p*I*	MW (kDa)	Ratio (T/N)	*p* value (*t* test)
1.1.1.1	P11766	Alcohol dehydrogenase 5 (class III), chi polypeptide (ADH5)	7.5	39.70	0.50	6.60E-05
4.2.1.11	P06733	Enolase 1 (ENO1)	7.4	47.14	1.59	2.60E-11
5.3.1.9	K7EQ48	Glucose-6-phosphate isomerase (GPI)	8.7	53.37	1.31	2.96E-02
1.2.1.12	P04406	Glyceraldehyde-3-phosphate dehydrogenase (GAPDH)	8.5	36.03	1.85	2.24E-44
1.1.1.27	P00338	Lactate dehydrogenase A (LDHA)	8.3	36.67	1.56	4.00E-04
1.1.1.27	P07195	Lactate dehydrogenase B (LDHB)	6.1	36.62	1.50	6.40E-03
2.7.1.11	Q01813	Phosphofructokinase, platelet (PFKP)	7.5	85.54	1.90	2.28E-02
2.7.1.40	A0A024R5Z9	Pyruvate kinase, muscle (PKM)	7.7	58.02	2.38	1.50E-04

Ratio (T/N) means the ratio of tumor to control

DEPs, differentially expressed proteins; *pI*, isoelectric point; *MW*, molecular weight

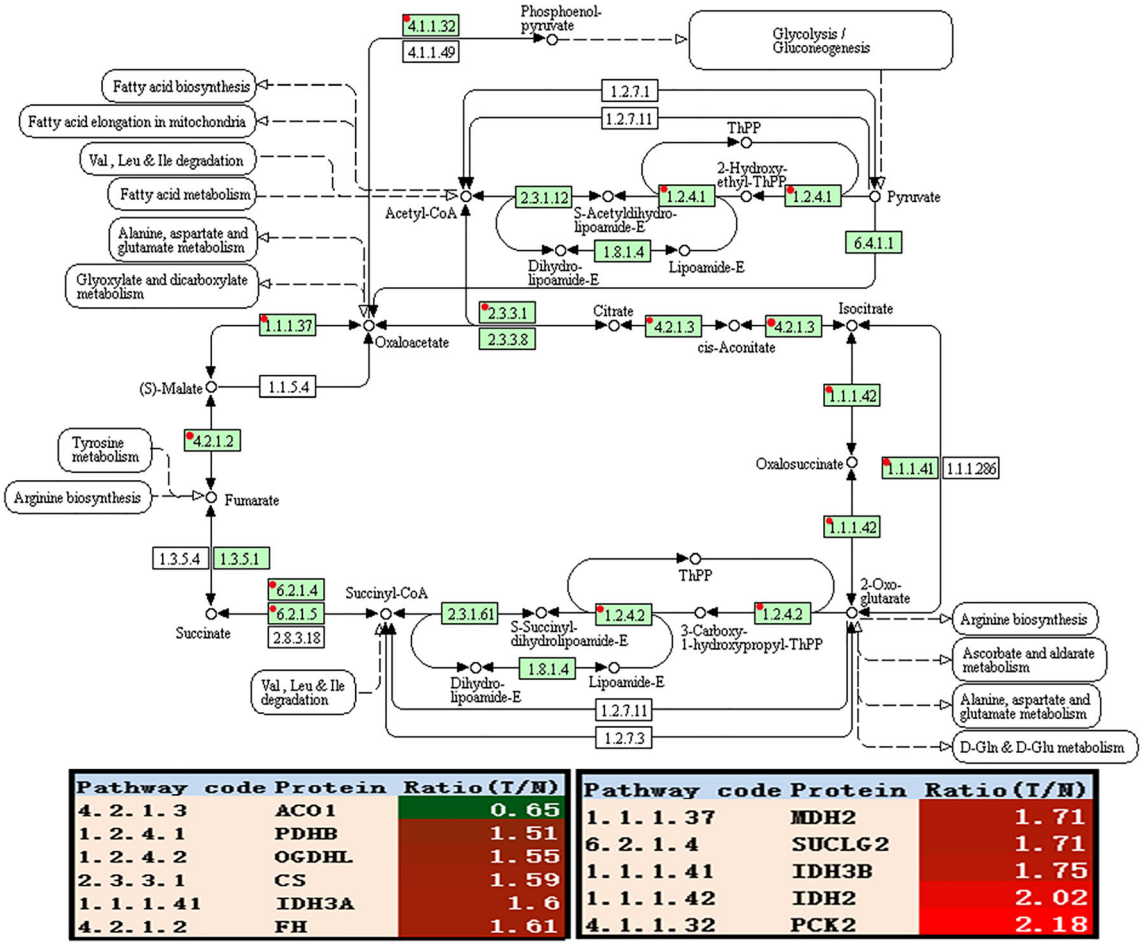

Fig. 3 Kreb's cycle altered in ovarian cancer. Green rectangle without red mark means species-specific enzymes. White rectangle means reference pathway. The solid line means molecular interaction. The dot line means indirect effect. The circle means mostly chemical complex. ACO1, cytoplasmic aconitate hydratase; PDHB, pyruvate dehydrogenase E1 subunit beta; IDH2, isocitrate dehydrogenase (NADP(+)) 2; CS, citrate synthase; IDH3A, mitochondrial isocitrate dehydrogenase [NAD] subunit alpha; FH, fumarate hydratase; MDH2, malate dehydrogenase 2; SUCLG2, succinate–CoA ligase GDP-forming subunit beta; IDH3B, isocitrate dehydrogenase (NAD(+)) 3 noncatalytic subunit beta; OGDHL, oxoglutarate dehydrogenase L; PCK2, mitochondrial phosphoenolpyruvate carboxykinase [GTP]

Table 4 Kreb's cycle involved mtDEPs operated in ovarian cancer biological system

Pathway code	Accession no.	Protein	Unique peptides	Coverage (%)	PSMs	Calc. p*I*	MW (kDa)	Ratio (T/N)	*p* value (*t* test)
4.2.1.3	P21399	Aconitase 1 (ACO1)	10	13.27	13	6.7	98.34	0.65	6.04E-03
4.1.1.32	Q16822	PCK2 protein (PCK2)	1	35.00	31	7.6	70.68	2.18	4.48E-03
1.2.4.1	P11177	Pyruvate dehydrogenase E1 component subunit beta, mitochondrial (PDHB)	14	52.92	79	6.7	39.21	1.51	3.25E-03
1.1.1.37	Q75MT9	Malate dehydrogenase (fragment) (MDH2)	21	74.37	262	8.3	33.21	1.71	5.51E-03
2.3.3.1	B4DJV2	Citrate synthase (CS)	13	26.93	73	7.9	50.40	1.59	4.65E-03
1.1.1.42	P48735	Isocitrate deh1ydrogenase (NADP), mitochondrial (IDH2)	27	56.64	355	8.7	50.88	2.02	2.07E-03
1.1.1.41	O43837	Isocitrate dehydrogenase (NAD) subunit beta, mitochondrial (IDH3B)	13	41.56	43	8.5	42.16	1.75	8.69E-03
1.1.1.41	P50213	Isocitrate dehydrogenase (NAD) subunit alpha, mitochondrial (IDH3A)	18	47.81	53	6.9	39.57	1.60	2.27E-02
4.2.1.2	P07954	Fumarate hydratase, mitochondrial (FH)	7	35.69	137	8.8	54.60	1.61	8.84E-03
6.2.1.4	Q96I99	Succinate–CoA ligase (GDP-forming) subunit beta, mitochondrial (SUCLG2)	19	44.91	115	6.4	46.48	1.71	8.17E-04
1.2.4.2	Q9ULD0	2-Oxoglutarate dehydrogenase-like, mitochondrial (OGDHL)	13	26.83	58	6.7	114.41	1.55	1.25E-03

Ratio (T/N) means the ratio of tumor to control

mtDEPs, mitochondrial differentially expressed proteins; *pI*, isoelectric point; *MW*, molecular weight; *PSMs*, peptide spectrum matches

IPA analysis indicated the association of the antiparasite drug ivermectin with production of ROS and energy metabolism

Disease and function analysis of ivermectin based on the IPA database showed that ivermectin was not only a broad-spectrum antiparasite drug but also associated with cancer treatment and production of ROS (Fig. 6a). Biomolecular network analysis of ivermectin based on the IPA database showed that ivermectin regulated enzymes (PKM, OGDHL, ND2, ND5, CytB, and UQCRH) in energy metabolism pathways through other molecules (Fig. 6b–g), which showed that ivermectin might have an impact on energy metabolism of cancer cells. Other molecules included the ivermectin directly regulated molecules such as CYP3A4, Rbp, GLRB, P2RX4, P2RX7, ABCB1, ABCG2, Abcb1b, P glycoprotein, cytokine, insulin, and strychnine, and the ivermectin indirectly regulated molecules such as APP, TNF, ERK1/2, MAPK1, MAPK13, MAPK3, NFKBIA, reactive oxygen species, STAT3, and testosterone (Supplementary Table 2).

Ivermectin-mediated key molecular changes in energy metabolism pathways of EOC

It is significant to explore ivermectin-mediated enzymes in energy metabolism pathways in EOCs. SILAC-based quantitative proteomics was used to analyze the protein expressions of energy metabolic pathways in ovarian cancer cells treated with (SILAC: H) and without (SILAC: L) 20 μM ivermectin for 24 h (Table 6). The results revealed that the glycolysis-related enzymes were significantly altered in EOC cells treated with vs. without ivermectin, including ADH5 (ratio H/L = 0.45, Q = 0.000), ENO1 (ratio H/L = 0.44, Q = 0.000), GPI (ratio H/L = 0.44, Q = 1.000), GAPDH (ratio H/L = /, which means the protein with expressed value 0 in both H and L groups; Q = 0.000), LDHA (ratio H/L = 0.34, Q = 1.000), LDHB (ratio H/L = 0.42, Q = 0.000), PFKP (ratio H/L = 0.54, Q = 0.000), and PKM (ratio H/L = +, which means the protein expressed in the H group but not in the L group; Q = 0.00745). The related enzymes of the Kreb's cycle were also significantly altered in EOC cells treated with vs. without ivermectin, including ACON (ratio H/L = −, which means the protein expressed in the L group but not in the H group; Q = 0.000), PCK2 (ratio H/L = 0.56, Q = 0.000), PDHB (ratio H/L = 0.46, Q = 0.000), MDH2 (ratio H/L = 0.42, Q = 0.000), CS (ratio H/L = 0.45, Q = 0.000), IDH2 (ratio H/L = 0.46, Q = 0.000), IDH3A (ratio H/L = 0.40, Q = 0.000), IDH3B (ratio H/L = 0.41, Q = 0.000), SUCLG2 (ratio H/L = 0.41, Q = 0.000), and OGDHL (ratio H/L = 0.56, Q = 0.000). The related enzymes of OXPHOS were also significantly altered in EOC cells treated with vs. without ivermectin, including CYTB (ratio H/L = 0.55, Q = 0.00359), UQCRH (ratio H/L = 0.51, Q = 0.000), COX17 (ratio H/L = 0.36, Q = 0.000), COX1 (ratio H/L = 0.38, Q = 0.000789), COX6C (ratio H/L = 0.34, Q = 0.000), COX4I1 (ratio H/L = 0.40, Q = 0.000), COX2 (ratio H/L = 0.38, Q = 0.000), COX7A2L (ratio H/L = 17.81, Q = 0.000534), COX7A2 (ratio H/L = 0.32, Q = 0.000), ATP6V0C (ratio H/L = 0.47, Q = 1.000), and ATP6 (ratio

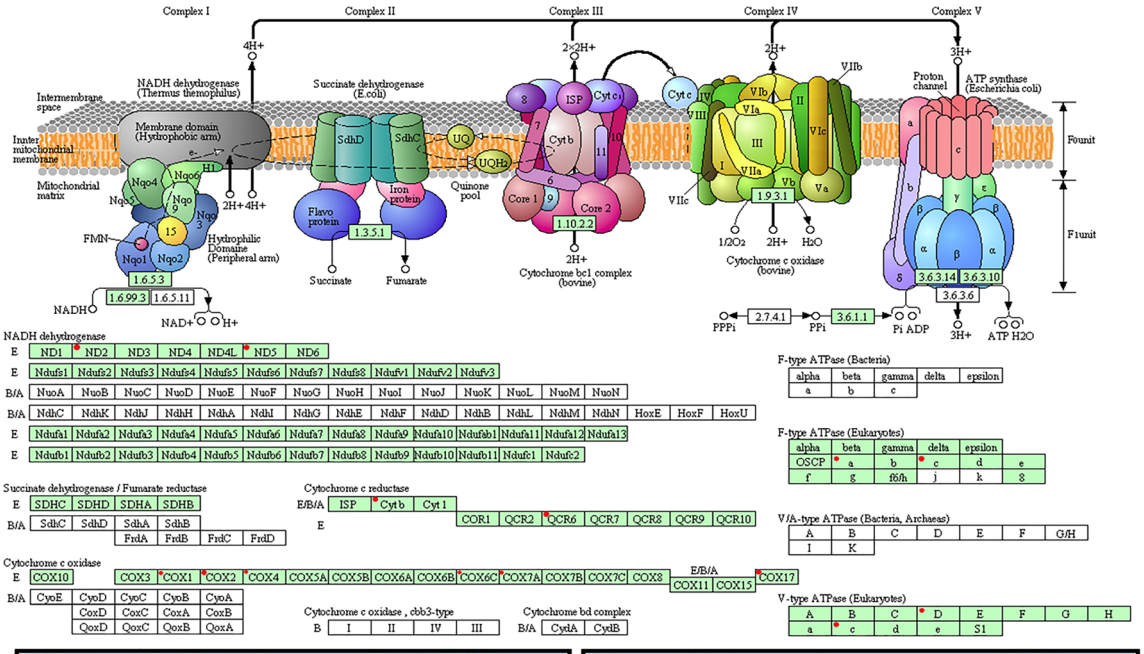

Pathway code	Protein	Ratio(T/N)
1.9.3.1	COX4I2	0.21
1.6.5.3	ND2	0.38
1.6.5.3	ND5	0.38
1.9.3.1	COX4I1	1.52
1.9.3.1	COX6C	1.54
3.6.3.1.4	ATP6V1D	1.54
1.9.3.1	COX7A2	1.55
3.6.3.1.4	ATP5G1	1.58
1.10.2.2	QCR6	1.59

Pathway code	Protein	Ratio(T/N)
3.6.3.1.4	ATP6V0C	1.63
1.9.3.1	COX2	1.68
1.10.2.2	cytb	1.71
1.9.3.1	COX1	1.79
3.6.3.1.4	ATP6	1.79
1.9.3.1	Fragment COX2	1.88
1.9.3.1	COX7A2L	1.88
1.9.3.1	COX17	2.75

Fig. 4 Oxidative phosphorylation altered in ovarian cancer. Green rectangle with red mark means the differential proteins. Green rectangle without red mark means species-specific enzymes. White rectangle means reference pathway. The solid line means molecular interaction. The dot line means indirect effect. The circle means mostly chemical complex. COX4I2, cytochrome *c* oxidase subunit 4I2; ND2, mitochondrially encoded NADH dehydrogenase 2; ND5, mitochondrially encoded NADH dehydrogenase 5; COX17, cytochrome *c* oxidase copper chaperone COX17; COX6C, cytochrome *c* oxidase subunit 6C; ATP6V1D, ATPase H+ transporting V1 subunit D; COX7A2, cytochrome *c* oxidase subunit 7A2; ATP5G1, ATP synthase membrane subunit c locus 1; QCR6, mitochondrial cytochrome b-c1 complex subunit 6; ATP6V0C, ATPase H+ transporting V0 subunit c; COX2, cytochrome *c* oxidase subunit II; CYTB, mitochondrially encoded cytochrome *b*; CYP3A4, cytochrome P450 family 3 subfamily A member 4; COX1, cytochrome *c* oxidase subunit; ATP6, ATP synthase F0 subunit 6; COX7A2L, cytochrome *c* oxidase subunit 7A2 like; COX4I1, cytochrome *c* oxidase subunit 4I1

H/L = 0.73, $Q = 0.000$). The lactate shuttle [MCT1 (ratio H/L = 0.53, $Q = 0.000$) and MCT4 (ratio H/L = 0.38, Q = 0.000)] were also changed in EOC cells treated with vs. without ivermectin.

Ivermectin inhibited the proliferation of EOC cells in vitro

The anticancer ability of ivermectin was measured with CCK8 assay before and after ivermectin treatment of EOC cells SKOV3 and TOV-21G and normal control cells IOSE80. After ivermectin treatment for 24 h, the viability of EOC cells was significantly decreased with an inhibition rate from 0, 28.1, 35.5, 64.9, 81.4, 93.7 to 93.8% for the control cells IOSE80; from 0, 5.6, 38.5, 87.1, 87.9, 88.2 to 90.7% for SKOV3; and from 0, 5.2, 33.6, 69.7, 82.1, 85.3 to 85.4% for TOV-21G, corresponding to the ivermectin concentration from 0, 10, 20, 30, 40 μM, 50 to 60 μM, which had a dose-dependent relationship (Fig. 7a). IC50 (29.46 μM) of the control cells IOSE80 was significantly higher than that of EOC cells (20.85 μM in SKOV3 and 22.54 in TOV-21G). Consistently, 20 μM ivermectin (which was close and slightly lower than their IC50) significantly suppressed cell proliferation in SKOV3 and TOV-21G cells as evidenced by CCK8 cell proliferation test (Fig. 7b, c), EdU cell proliferation test (Fig. 7d–f), and reduced clonogenic survival (Fig. 7g, h) in ivermectin-treated cells compared with controls (0 μM ivermectin), which had a time-dependent relationship (Fig. 7b, c). Further analysis found that 10 μM ivermectin (which was much lower than their IC50) did not suppress cell proliferation in SKOV3 and TO-21G cells (Fig. 7b–h), and 30 μM ivermectin (which was much higher than their IC50) caused cell death in SKOV3 and TO-21G cells (Fig. 7d–h). These results clearly demonstrated that 20 μM ivermectin was a suitable dose and significantly inhibited in vitro proliferation and growth of ovarian cancer cells.

Table 5 Oxidative phosphorylation involved mtDEPs operated in ovarian cancer biological system

Pathway code	Accession no.	Protein	Unique peptides	Coverage (%)	PSMs	Calc. p*I*	MW (kDa)	Ratio (T/N)	*p* value (*t* test)
1.6.5.3	A0A059T3A1	NADH-ubiquinone oxidoreductase chain 2 (ND2)	1	4.61	2	9.8	38.93	0.38	6.03E-04
1.6.5.3	A0A096WB60	NADH-ubiquinone oxidoreductase chain 5 (ND5)	1	5.14	6	9.0	67.01	0.38	3.34E-04
1.10.2.2	A0A0A0QN99	Cytochrome *b* (cytb)	1	4.21	4	8.0	42.71	1.71	7.60E-03
1.10.2.2	P07919	Cytochrome b-c1 complex subunit 6, mitochondrial (QCR6)	5	51.65	18	4.4	10.73	1.59	1.63E-02
1.9.3.1	H7C4E5	COX17, cytochrome *c* oxidase copper chaperone (COX17)	1	12.07	1	7.7	6.41	2.75	2.33E-03
1.9.3.1	H9LP39	Cytochrome *c* oxidase subunit I (COX1)	1	6.04	1	6.7	57.01	1.79	2.44E-03
1.9.3.1	P09669	Cytochrome *c* oxidase subunit 6C (COX6C)	7	52	30	10.4	8.78	1.54	5.97E-03
1.9.3.1	Q96KJ9	Cytochrome *c* oxidase subunit 4I2 (COX4I2)	1	5.85	1	9.6	20.00	0.21	6.28E-04
1.9.3.1	P13073	Cytochrome *c* oxidase subunit 4 isoform 1, mitochondrial (COX4I1)	7	36.09	48	9.5	19.56	1.52	4.37E-03
1.9.3.1	A0A097Q0T5	Cytochrome *c* oxidase subunit 2 (COX2)	1	26.43	64	4.8	25.55	1.68	4.38E-02
1.9.3.1	H9E7B8	Cytochrome *c* oxidase subunit 2 (fragment) (COX2)	1	27.27	65	4.7	24.84	1.88	1.97E-02
1.9.3.1	O14548	Cytochrome *c* oxidase subunit 7A2 like (COX7A2L)	4	54.39	8	9.4	12.61	1.88	5.33E-03
1.9.3.1	P14406	Cytochrome *c* oxidase subunit 7A2 (COX7A2)	2	27.71	15	9.8	9.39	1.55	3.89E-02
3.6.3.1.4	P27449	ATPase H+ transporting V0 subunit c (ATP6V0C)	1	11.61	18	8.4	15.73	1.63	4.24E-04
3.6.3.1.4	A0A059QB80	ATP synthase subunit a (ATP6)	1	4.42	17	10.1	24.74	1.79	6.63E-03
3.6.3.1.4	G3V2V6	ATPase H+ transporting V1 subunit D (ATP6V1D)	1	7.43	1	9.5	17.41	1.54	8.22E-04
3.6.3.1.4	I3L0Y5	ATP synthase, H+ transporting, mitochondrial Fo complex subunit C1 (subunit 9) (ATP5G1)	1	7.14	6	10.0	10.03	1.58	9.78E-03

Ratio (T/N) means the ratio of tumor to control

mtDEPs, mitochondrial differentially expressed proteins; *pI*, isoelectric point; *MW*, molecular weight; *PSMs*, peptide spectrum matches

Ivermectin inhibited cell cycle progression and promoted EOC cell apoptosis

To gain insights into the mechanism that ivermectin inhibited EOC cell proliferation, differences in cell cycle distributions were analyzed after treatments with different concentrations of ivermectin (0, 10, 20, and 30 μM) for 24 h with fluorescence-activated cell sorting (FACS). The results found that significant G0/G arrest was observed in the high drug concentration (20 μM and 30 μM) groups compared with the control (0 μM) and low drug concentration (10 μM) groups (Fig. 8a–c) and that the proportion of cells was significantly increased in G0/G phase, significantly decreased in S phase, and no change in G2/M phase in the 20- and 30-μM ivermectin groups compared with the 0- and 10-μM ivermectin groups (Fig. 8b, c). These data strongly demonstrated that ivermectin inhibited cell proliferation by blocking cell cycle progression from G0/G to S phase. Furthermore, the apoptosis was measured with FACS in EOC cells that were stained with PI and annexin V. The results showed that the proportion of apoptosis cells was significantly increased in the 10-, 20-, and 30-μM drug concentration groups compared with the control (0 μM) groups, and the proportion of apoptosis cells was increased with the increased drug concentrations (Fig. 8d, e). These findings clearly demonstrated that ivermectin inhibited EOC cell cycle progression from G0/G to S phases and promoted its apoptosis.

Fig. 5 Western blot analysis to validate results of iTRAQ labeling. **a**, **b** ▶ Mitochondrial proteins of EOC and control tissues were analyzed by WB using antibodies against PKM2, PDHB, CS, IDH2, OGDHL, and UQCRH. The levels of PKM2, PDHB, CS, IDH2, OGDHL, and UQCRH were normalized relative to β-actin. Data represent mean values ± SD. **c** Warburg effect and the reverse Warburg effect. Parenchymal cells showed metabolic heterogeneity. Some cancer cells were high glycolytic cancer cell consisting with "Warburg effect," and the other cancer cells were oxidative cancer cell consisting with "the reverse Warburg effect." Tumor cells and stroma cells (especially CAFs) have metabolic symbiosis; thus, cancer cell induced oxidative stress of CAFs by secreting ROS and enhanced aerobic glycolysis in CAFs. In turn, CAFs produced lots of nourishment, which was "eaten" up by the cancer cells to produce ATP. $*p < 0.05$, $**p < 0.01$, $***p < 0.001$. iTRAQ, isobaric tags for relative and absolute quantitation; EOC, epithelial ovarian carcinoma; WB, western blot; ROS, reactive oxygen species; PKM2, pyruvate kinase M2; PDHB, pyruvate dehydrogenase E1 subunit beta; CS, citrate synthase; IDH2, isocitrate dehydrogenase (NADP(+)) 2; OGDHL, oxoglutarate dehydrogenase L; UQCRH, ubiquinol-cytochrome *c* reductase hinge protein; CAFs, cancer-associated fibroblasts; PDK, pyruvate dehydrogenase (acetyl-transferring)] kinase; MCT1, solute carrier family 16 member 1; MCT4, solute carrier family 16 member 4

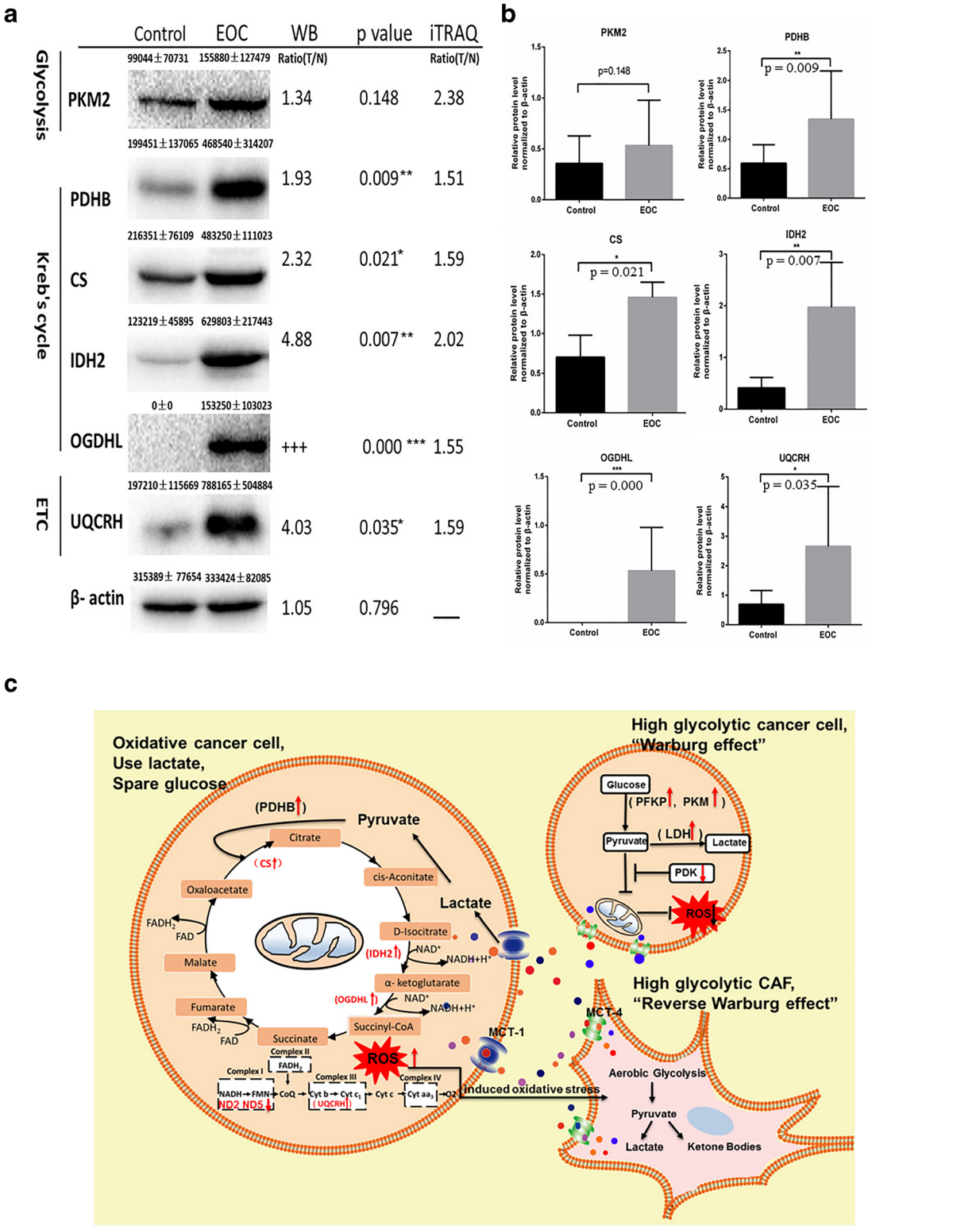
a
Control
EOC
WB
p value
iTRAQ
Glycolysis
PKM2
99044±70731
155880±127479
Ratio(T/N)
Ratio(T/N)
1.34
0.148
2.38
PDHB
199451±137065
468540±314207
1.93
0.009**
1.51
Kreb's cycle
CS
216351±76109
483250±111023
2.32
0.021*
1.59
IDH2
123219±45895
629803±217443
4.88
0.007**
2.02
OGDHL
0±0
153250±103023
+++
0.000 ***
1.55
ETC
UQCRH
197210±115669
788165±504884
4.03
0.035*
1.59
β- actin
315389± 77654
333424±82085
1.05
0.796
b
PKM2
p=0.148
PDHB
p = 0.009
CS
p = 0.021
IDH2
p = 0.007
OGDHL
p = 0.000
UQCRH
p = 0.035
Relative protein level normalized to β-actin
Control
EOC
c
Oxidative cancer cell,
Use lactate,
Spare glucose
(PDHB↑)
Pyruvate
Citrate
(CS↑)
cis-Aconitate
Oxaloacetate
Lactate
FADH2
FAD
D-Isocitrate
(IDH2↑)
NAD+
NADH+H+
Malate
α- ketoglutarate
(OGDHL↑)
NAD+
NADH+H+
Fumarate
FADH2
FAD
Succinyl-CoA
Succinate
MCT-1
Complex II
FADH2
ROS
Complex I
Complex III
Complex IV
NADH→FMN→CoQ→Cyt b→Cyt c1→Cyt c→Cyt aa3→O2
ND2 ND5
(UQCRH↓)
induced oxidative stress
High glycolytic cancer cell,
"Warburg effect"
Glucose
(PFKP↑, PKM↑)
Pyruvate
(LDH↑)
Lactate
PDK↓
ROS↑
High glycolytic CAF,
"Reverse Warburg effect"
MCT-4
Aerobic Glycolysis
Pyruvate
Lactate
Ketone Bodies
d
IOSE80
SK-OV3
WB
p value
650101±10731
720748±97479
Ratio(T/N)
MCT1
1.10
0.941
843885±17065
1824268±214207
MCT4
2.16
0.003
β- actin
IOSE80
TOV-21G
WB
p value
1042234±98409
1805705±166023
Ratio(T/N)
1.73
0.038
565377±10114
2464762±703821
4.35
0.000
Control
EOC
WB
p value
216351±76109
Ratio(T/N)
+++
0.000
216351±76109
+++
0.000

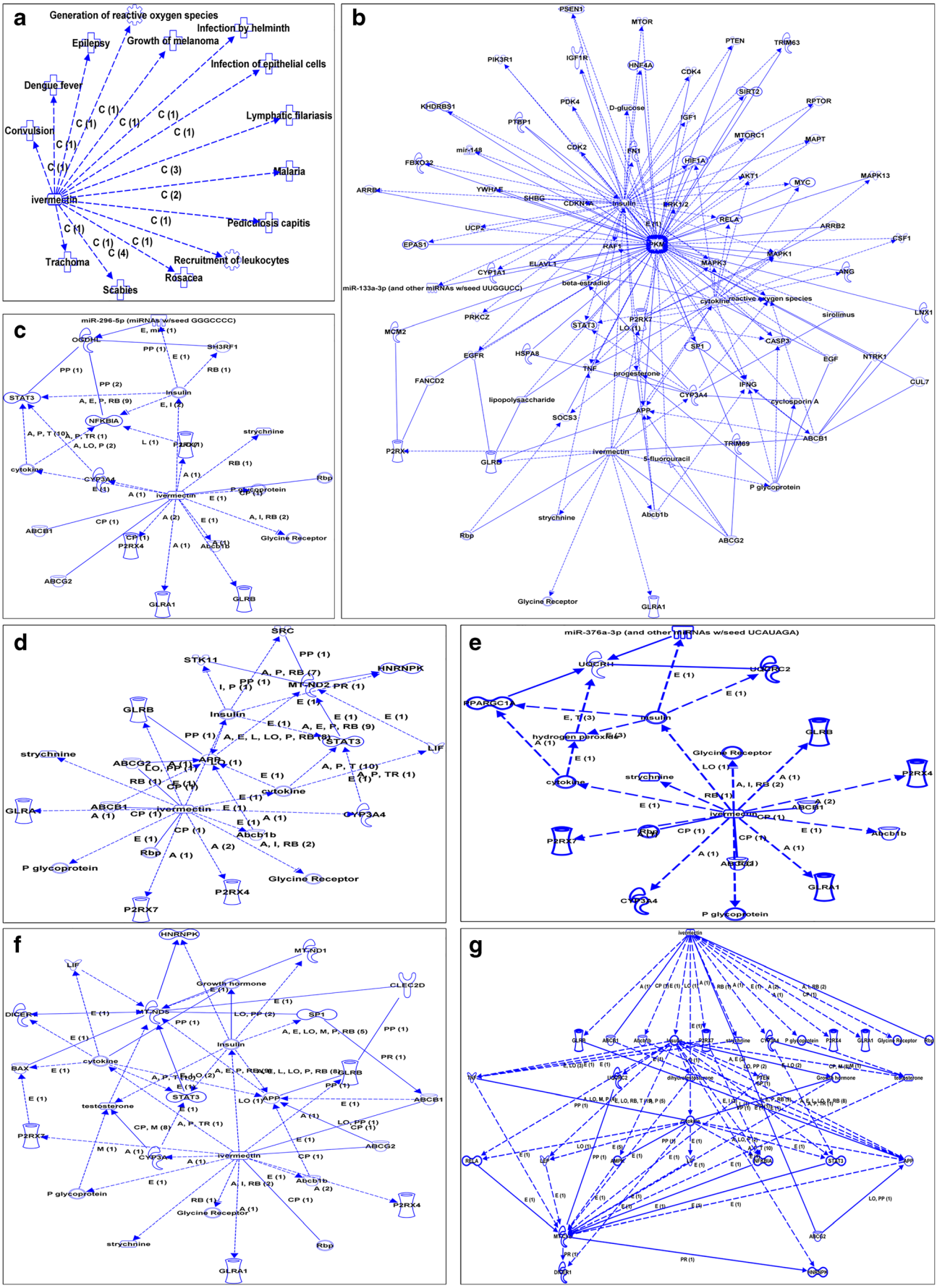
a
Generation of reactive oxygen species
Infection by helminth
Epilepsy
Growth of melanoma
Infection of epithelial cells
Dengue fever
Lymphatic filariasis
Convulsion
Malaria
ivermectin
Pediculosis capitis
Recruitment of leukocytes
Trachoma
Rosacea
Scabies
b
PSEN1
MTOR
PTEN
TRIM63
PIK3R1
IGF1R
HNF4A
CDK4
SIRT2
RPTOR
KHDRBS1
PDK4
D-glucose
PTBP1
IGF1
MTORC1
MAPT
mir-148
CDK2
FN1
HIF1A
FBXO32
AKT1
MYC
MAPK13
ARRB1
YWHAE
SHBC
CDKN1A
insulin
MAPK3/2
RELA
ARRB2
UCP2
EPAS1
RAF1
AKT
CSF1
ELAVL1
MAPK1
CYP1A1
ANG
miR-133a-3p (and other miRNAs w/seed UUGGUCC)
beta-estradiol
cytokine
reactive oxygen species
sirolimus
LNX1
PRKCZ
STAT3
P2RK7
LO (1)
MCM2
CASP3
SP1
EGFR
HSPA8
EGF
NTRK1
TNF
progesterone
FANCD2
CUL7
IFNG
lipopolysaccharide
CYP3A4
cyclosporin A
SOCS3
APP
ABCB1
P2RX4
TRIM69
GLRB
ivermectin
5-fluorouracil
P glycoprotein
strychnine
Abcb1b
Rbp
ABCG2
Glycine Receptor
GLRA1
c
miR-296-5p (miRNAs w/seed GGGCCCC)
OGDHL
SH3RF1
PP (1)
E (1)
RB (1)
PP (2)
STAT3
Insulin
A, E, P, RB (9)
E, I (2)
NFKBIA
A, P, T (10)
A, P, TR (1)
A, LO, P (2)
L (1)
P2RX7
strychnine
cytokine
RB (1)
CYP3A4
E (1)
A (1)
Rbp
P glycoprotein
CP (1)
ivermectin
A, I, RB (2)
ABCB1
A (2)
Glycine Receptor
P2RX4
ABCG2
GLRA1
GLRB
d
SRC
PP (1)
STK11
A, P, RB (7)
HNRNPK
I, P (1)
MT-ND2 PR (1)
E (1)
GLRB
Insulin
A, E, P, RB (9)
PP (1)
A, E, L, LO, P, RB (8)
STAT3
LIF
strychnine
ABCG2
LO, PP (1)
ABCB1
A, P, T (10)
RB (1)
A, P, TR (1)
cytokine
GLRA1
ABCB1
ivermectin
CYP3A4
A (1)
CP (1)
Abcb1b
A, I, RB (2)
Rbp
P glycoprotein
P2RX4
Glycine Receptor
P2RX7
e
miR-376a-3p (and other miRNAs w/seed UCAUAGA)
UQCRH
UQCRC2
PPARGC1A
E, T (3)
insulin
hydrogen peroxide
GLRB
Glycine Receptor
strychnine
LO (1)
P2RX4
cytokine
A, I, RB (2)
RB (1)
ABCB1
ivermectin
CP (1)
Abcb1b
P2RX7
Rbp
GLRA1
CYP3A4
P glycoprotein
f
HNRNPK
MT-ND1
LIF
Growth hormone
CLEC2D
DICER1
MT-ND5
SP1
LO, PP (2)
Insulin
BAX
cytokine
A, E, P, RB (9)
A, E, L, LO, P, RB (8)
GLRB
STAT3
APP
ABCB1
testosterone
P2RX7
CP, M (8)
A, P, TR (1)
CYP3A4
ivermectin
ABCG2
P glycoprotein
Abcb1b
A, I, RB (2)
Glycine Receptor
P2RX4
strychnine
Rbp
GLRA1
g
ivermectin
GLRB
ABCB1
Abcb1b
P2RX7
strychnine
CYP3A4
P glycoprotein
P2RX4
GLRA1
Glycine Receptor
TNF
UQCRC2
dihydrotestosterone
PTEN
Growth hormone
testosterone
Insulin
RELA
STAT3
APP
MYC
ABCG2
DICER1
INSR

◀ **Fig. 6** IPA analysis revealed that ivermectin was associated with production of ROS and energy metabolism. **a** Disease and function analysis of ivermectin based on IPA software. **b** Biomolecular networks analysis of ivermectin based on IPA software showed that ivermectin regulated PKM. **c** Biomolecular networks analysis of ivermectin based on IPA software showed that ivermectin regulated OGDHL. **d** Biomolecular networks analysis of ivermectin based on IPA software showed that ivermectin regulated ND2. **e** Biomolecular networks analysis of ivermectin based on IPA software showed that ivermectin regulated ND5. **f** Biomolecular networks analysis of ivermectin based on IPA software showed that ivermectin regulated UQCRH. IPA, Ingenuity Pathway Analysis; ROS, reactive oxygen species; PKM, pyruvate kinase muscle; OGDHL, oxoglutarate dehydrogenase L; ND2, mitochondrially encoded NADH dehydrogenase 2; ND5, mitochondrially encoded NADH dehydrogenase 5; UQCRH, ubiquinol-cytochrome *c* reductase hinge protein

Ivermectin affected energy metabolism pathways for its anticancer effects through targeting PFKP, IDH2, IDH3B, ND2, ND5, CYTB, UQCRH, MCT1, and MCT4 in the energy metabolism pathways

To further investigate the molecular mechanisms that ivermectin inhibited proliferation and promoted apoptosis in EOC cells, EOC cells treated with ivermectin (10 μM, 20 μM, and 30 μM) and control cells (within 0.1% DMSO) were established. The mRNA expressions of target genes (PFKP, PKM, CS, PDHB, IDH2, IDH3A, IDH3B, OGDHL, ND2, ND5, CYTB, UQCRH, MCT1, and MCT4) were analyzed by qRT-PCR (Fig. 9a–f). A significant change was found for the mRNA expressions of target genes in energy metabolism pathways. Furthermore, western blot revealed that the protein expressions of target genes were significantly changed in ivermectin-treated EOC cells, including PFKP, IDH2, IDH3A, IDH3B, ND2, ND5, CYTB, UQCRH, MCT1, and MCT4 (Fig. 10). For the first time, these findings clearly demonstrated that ivermectin significantly changed the expressions of key molecules in energy metabolism pathways, which indicated that ivermectin might regulate ovarian cancer energy metabolism pathways.

Discussion

EOC is a type of ovarian malignant neoplasms with high mortality in women and unclear molecular mechanisms [50]. Cancer cell metabolism alteration became one of the research hot spots. Cancer cells in tumor tissues are highly heterogeneous. For tumor energy metabolism, the coexistence of Warburg and reverse Warburg effects in cancer tissues has become the common sense [20, 24, 27]. However, the landscape of detailed molecular profiling changes in energy metabolism pathways remains unclear in EOC. This study made the advances in clarifying the molecular profiling changes in EOC energy metabolism pathways, including glycolysis, Kreb's cycle, oxidative phosphorylation, and lactate shuttle.

Cancer cells needed more fuel to maintain high growth rate compared with normal cells [51]. In 1956, Warburg found that the principal energy supplies of cancer cells were from aerobic glycolysis [21]. "Warburg effect" played a leading role for energy generations in cancer cells, and many researchers were engaged in developing drugs against the anti-Warburg effect. It is well-known that splicing and posttranslational modifications (PTMs) were tightly associated with diseases [52, 53]. PKM2 was closely related to energy metabolic reprogramming, because the activity of PKM2 was regulated by many ways including PTMs [54]. PKM2 might be associated with the Warburg effect. It was reported that PKM2 modification might lead to increased glucose consumption [22]. Thus, anti-Warburg effect drugs would be potential inhibitors for cancer treatment. For example, one kind of anti-Warburg effect agents, the erastin-like agent, could effectively decrease lactate formation in cancer cells to prevent mitochondrial depolarization [55].

However, the interactions between cancer cells and stromal cells, or cancer cells and cancer cells, were completely ignored according to the Warburg effect. The reverse Warburg effect took into consideration the tumor microenvironment, which complemented the Warburg effect in terms of energy metabolism. In the novel reverse Warburg effect model, energy metabolism involved high aerobic glycolysis in cancer cells and the neighboring stromal fibroblasts and increasing OXPHOS process in other cancer cells. The interaction among those cells relied on the "lactate shuttle" (MCT1 and MCT4). Energy-rich metabolites were transported through the "lactate shuttle" from high aerobic glycolysis cells to increasing OXPHOS cancer cells [24]. Thus, the coexistence of the Warburg effect and reverse Warburg effect made the regulatory mechanism of energy metabolism more reasonable. The Warburg effect and reverse Warburg effect could not suppress each other, and the new reverse Warburg effect theory could not replace the Warburg effect. In a word, the coexistence of two effects reflected the heterogeneity and plasticity of energy metabolism in cancer [56]. The detailed mechanisms of energy metabolism heterogeneity still remain unclear. The questions were as follows: How was the metabolic coupling processed? Which was competing for the leading role in the cancer energy metabolism? What kind of drugs could block both the Warburg and reverse Warburg effects?

This study found that many key protein molecules were significantly changed in three energy metabolism pathways (glycolysis, Kreb's cycle, and OXPHOS) in EOC. Interestingly, the results demonstrated the enhanced ability of those three energy pathways for ATP generation, with the upregulation of rate-limiting enzyme subunits (PKM, CS, IDH2, and OGDHL). Furthermore, immunoaffinity experiments confirmed the upregulated PKM2 in the glycolysis

Table 6 SILAC-based quantitative proteomics analysis of the protein expressions of energy metabolic pathways in ovarian cancer cells TOV-21G treated with (SILAC: H) and without (SILAC: L) 20 μM ivermectin for 24 h, and verified with qPCR and western blot

Pathway	Protein ID	Gene name	Protein name	Peptides	Unique peptides	Sequence coverage [%]	Mol. weight [kDa]	Sequence length	Score	*Q* value	Intensity H	Intensity L	Ratio H/L
Glycolysis pathway	PFKAP	PFKP	ATP-dependent 6-phosphofructokinase, platelet type	31	28	46.7	85.6	784	323.3	0.00E+00	14,226,000,000	25,587,000,000	0.54
	H3BQ34	PKM	Pyruvate kinase	1	1	0.0	30.7	281	1.9	7.46E-03	10,727,000	0	+
	ODPB	PDHB	Pyruvate dehydrogenase E1 component subunit beta, mitochondrial	9	9	34.0	39.2	359	67.1	0.00E+00	407,280,000	1,649,500,000	0.46
	K4EN11	GAPDH	GAPDH (fragment)	1	1	48.1	2.8	27	6.3	0.00E+00	0	0	/
	ENOA	ENO1	Alpha-enolase	21	11	65.9	47.2	434	323.3	0.00E+00	54,687,000,000	125,660,000,000	0.44
	F5GXY2	LDHA	L-lactate dehydrogenase A chain (fragment)	15	1	82.1	17.3	156	− 2.0	1.00E+00	10,379,000	29,470,000	0.34
	Q5U077	LDHB	L-lactate dehydrogenase	17	8	49.4	36.6	334	160.4	0.00E+00	27,852,000,000	66,990,000,000	0.42
	A0A0A0MTS2	GPI	Glucose-6-phosphate isomerase (fragment)	21	1	48.0	64.8	573	− 2.0	1.00E+00	56,685,000	138,520,000	0.44
	Q6IRT1	ADH5	S-(hydroxymethyl)glutathione dehydrogenase	16	16	52.9	39.7	374	115.0	0.00E+00	1,308,100,000	3,513,700,000	0.45
	B3KUV2	ACSS2	cDNA FLJ40707 fis, clone THYMU2026835, highly similar to acetyl-coenzyme A synthetase, cytoplasmic	2	2	6.6	45.5	409	1.8	9.53E-03	9,455,200	25,758,000	0.73
	H3BRS6	ADPGK	ADP-dependent glucokinase (fragment)	2	2	13.2	21.8	204	3.1	5.31E-04	11,465,000	18,413,000	0.69
	AL1B1	ALDH1B1	Aldehyde dehydrogenase X, mitochondrial	6	5	17.0	57.2	517	26.0	0.00E+00	69,821,000	196,750,000	0.45
	ALDH2	ALDH2	Aldehyde dehydrogenase, mitochondrial	18	17	48.4	56.4	517	68.0	0.00E+00	812,240,000	1,822,600,000	0.44
	AL3A2	ALDH3A2	Aldehyde dehydrogenase family 3 member A2	10	10	26.0	51.9	461	30.5	0.00E+00	225,000,000	394,360,000	0.55
	AL9A1	ALDH9A1	4-Trimethylaminobutyraldehyde dehydrogenase	18	18	39.3	53.8	494	77.3	0.00E+00	529,020,000	1,322,400,000	0.48
	A0A024QZ64	ALDOC	Fructose-bisphosphate aldolase	12	8	45.1	39.5	364	109.3	0.00E+00	1,104,800,000	2,650,700,000	0.43
	H0YDD4	DLAT	Acetyltransferase component of pyruvate dehydrogenase complex (fragment)	8	8	21.1	51.2	479	74.8	0.00E+00	530,720,000	1,251,100,000	0.46
	A0A024R713	DLD	Dihydrolipoyl dehydrogenase	13	13	37.7	48.9	459	35.1	0.00E+00	632,170,000	1,843,800,000	0.52
	Q6FHV6	ENO2	ENO2 protein	13	11	50.2	47.3	434	175.6	0.00E+00	618,190,000	2,887,100,000	0.26
	ENOB	ENO3	Beta-enolase	4	2	19.4	47.0	434	6.7	0.00E+00	215,810,000	482,340,000	0.59
	B4DG62	HK1	cDNA FLJ56506, highly similar to hexokinase-1	29	22	36.0	102.3	915	109.9	0.00E+00	1,617,000,000	4,075,800,000	0.53
	HKDC1	HKDC1	Hexokinase HKDC1	15	11	17.7	102.5	917	57.9	0.00E+00	132,850,000	568,430,000	0.30

Table 6 (continued)

Pathway	Protein ID	Gene name	Protein name	Peptides	Unique peptides	Sequence coverage [%]	Mol. weight [kDa]	Sequence length	Score	*Q* value	Intensity H	Intensity L	Ratio H/L
	PCKGC	PCK1	Phosphoenolpyruvate carboxykinase, cytosolic [GTP]	8	6	17.0	69.2	622	15.3	0.00E+00	1,267,700	160,370,000	0.07
	A0A384MTT2	PCK2	Epididymis secretory sperm binding protein	12	10	25.8	70.7	640	61.9	0.00E+00	403,190,000	1,032,500,000	0.56
	A0A024RBX9	PDHA1	Pyruvate dehydrogenase E1 component subunit alpha	11	11	35.1	43.3	390	102.8	0.00E+00	457,490,000	1,353,000,000	0.49
	PFKAL	PFKL	ATP-dependent 6-phosphofructokinase, liver type	16	12	27.1	85.0	780	161.1	0.00E+00	1,242,500,000	2,567,300,000	0.52
	A0A024R0Y5	PFKM	ATP-dependent 6-phosphofructokinase	20	17	35.5	85.2	780	323.3	0.00E+00	1,677,600,000	3,768,800,000	0.47
	Q6P6D7	PGAM1	Phosphoglycerate mutase	15	15	70.5	28.8	254	226.1	0.00E+00	11,906,000,000	30,409,000,000	0.36
	A0A3B3ITK7	PGM1	Phosphoglucomutase-1	18	18	40.2	64.0	584	109.1	0.00E+00	721,450,000	1,641,900,000	0.43
	PGM2	PGM2	Phosphoglucomutase-2	9	9	19.8	68.3	612	13.7	0.00E+00	144,180,000	423,580,000	0.40
	A0A024R5Z9	PKM2	Pyruvate kinase	39	1	71.6	58.1	531	− 2.0	1.00E+00	35,541,000	125,430,000	0.54
Kreb's cycle	ODPB	PDHB	Pyruvate dehydrogenase E1 component subunit beta, mitochondrial	9	9	34.0	39.2	359	67.1	0.00E+00	407,280,000	1,649,500,000	0.46
	B4DJV2	CS	Citrate synthase	15	14	43.0	50.4	453	76.8	0.00E+00	2,428,500,000	5,338,700,000	0.45
	IDHP	IDH2	Isocitrate dehydrogenase [NADP], mitochondrial	18	17	48.0	50.9	452	174.3	0.00E+00	1,281,200,000	2,994,300,000	0.46
	IDH3A	IDH3A	Isocitrate dehydrogenase [NAD] subunit alpha, mitochondrial	10	10	36.4	34.5	316	90.6	0.00E+00	268,600,000	1,119,300,000	0.40
	A0A087WZN1	IDH3B	Isocitrate dehydrogenase [NAD] subunit, mitochondrial	8	8	26.6	42.4	387	26.8	0.00E+00	142,630,000	477,180,000	0.41
	OGDHL	OGDHL	2-Oxoglutarate dehydrogenase-like, mitochondrial	10	5	10.9	114.5	1010	12.7	0.00E+00	17,707,000	119,970,000	0.56
	O75944	ACON	Aconitase (fragment)	16	3	33.5	65.3	600	12.1	0.00E+00	0	48,304,000	–
	A0A384MTT2	PCK2	Epididymis secretory sperm binding protein	12	10	25.8	70.7	640	61.9	0.00E+00	403,190,000	1,032,500,000	0.56
	Q0QF37	MDH2	Malate dehydrogenase (fragment)	17	17	70.5	32.0	305	323.3	0.00E+00	5,856,200,000	14,406,000,000	0.42
	A0A024R325	SUCLG2	Succinate–CoA ligase [GDP-forming] subunit beta, mitochondrial	8	8	25.5	46.5	432	42.3	0.00E+00	232,210,000	779,800,000	0.41
	Q71UF1	ACO2	Aconitate hydratase, mitochondrial	24	0	38.6	85.6	780	− 2.0	1.00E+00	0	12,950,000	–
	A0A024R1Y2	ACLY	ATP-citrate synthase	37	37	42.4	119.8	1091	183.5	0.00E+00	2,033,900,000	4,490,700,000	0.46
	H0YDD4	DLAT	Acetyltransferase component of pyruvate dehydrogenase complex (fragment)	8	8	21.1	51.2	479	74.8	0.00E+00	530,720,000	1,251,100,000	0.46
	A0A024R713	DLD	Dihydrolipoyl dehydrogenase	13	13	37.7	48.9	459	35.1		632,170,000	1,843,800,000	0.52

Table 6 (continued)

Pathway	Protein ID	Gene name	Protein name	Peptides	Unique peptides	Sequence coverage [%]	Mol. weight [kDa]	Sequence length	Score	*Q* value	Intensity H	Intensity L	Ratio H/L
										0.00E+00			
	Q6IBS5	DLST	DLST protein	7	7	20.5	48.8	453	44.5	0.00E+00	601,540,000	1,338,700,000	0.53
	A0A0S2Z4C3	FH	Epididymis secretory sperm binding protein (fragment)	14	14	35.5	54.6	510	161.7	0.00E+00	1,498,700,000	3,849,500,000	0.43
	IDH3G	IDH3G	Isocitrate dehydrogenase [NAD] subunit gamma, mitochondrial	7	7	27.7	42.8	393	42.3	0.00E+00	55,446,000	230,380,000	0.54
	ODO1	OGDH	2-Oxoglutarate dehydrogenase, mitochondrial	23	18	31.5	115.9	1023	82.1	0.00E+00	325,090,000	949,610,000	0.43
	A0A494C101	PC	Pyruvate carboxylase, mitochondrial (fragment)	2	2	5.2	53.5	483	3.0	7.83E-04	3,454,600	19,685,000	0.28
	PCKGC	PCK1	Phosphoenolpyruvate carboxykinase, cytosolic [GTP]	8	6	17.0	69.2	622	15.3	0.00E+00	1,267,700	160,370,000	0.07
	A0A024RBX9	PDHA1	Pyruvate dehydrogenase E1 component subunit alpha	11	11	35.1	43.3	390	102.8	0.00E+00	457,490,000	1,353,000,000	0.49
	A0A024QZ30	SDHA	Succinate dehydrogenase [ubiquinone] flavoprotein subunit, mitochondrial	20	20	44.9	72.7	664	200.0	0.00E+00	1,096,500,000	2,950,800,000	0.44
	SDHB	SDHB	Succinate dehydrogenase [ubiquinone] iron-sulfur subunit, mitochondrial	6	2	24.3	31.6	280	17.3	0.00E+00	143,030,000	516,360,000	0.37
	D3DVH1	SDHC	Succinate dehydrogenase complex, subunit C, integral membrane protein, 15 kDa, isoform CRAa	3	3	35.2	11.3	105	6.8	0.00E+00	68,060,000	130,150,000	0.46
	B7ZAF6	SUCLA2	Succinate–CoA ligase [ADP-forming] subunit beta, mitochondrial	9	9	36.2	36.0	329	127.1	0.00E+00	114,900,000	726,200,000	0.33
	Q6IAL5	SUCLG1	Succinate–CoA ligase [ADP/GDP-forming] subunit alpha, mitochondrial	8	8	30.3	35.0	333	45.9	0.00E+00	261,580,000	1,105,700,000	0.34
Oxidative phosphorylation	D2Y6X2	ND5	NADH dehydrogenase subunit 5 (fragment)	1	1	26.8	4.5	41	3.2	5.33E-04	4,125,200	24,591,000	0.41
	A0A1B0TCA9	CYTB	Cytochrome *b* (fragment)	1	1	2.8	35.7	318	2.2	3.59E-03	53,396,000	59,765,000	0.55
	Q567R0	UQCRH	UQCRH protein	1	1	21.2	10.0	85	37.0	0.00E+00	252,050,000	546,900,000	0.51
	C9J8T6	COX17	Cytochrome *c* oxidase copper chaperone	1	1	16.3	10.9	98	3.5	0.00E+00	7,643,200	53,020,000	0.36
	Q6FGA0	COX7A2L	COX7A2L protein	2	2	19.3	12.6	114	3.2	5.34E-04	22,802,000	1,280,400	17.81
	U3L4G0	ATP6	ATP synthase subunit a	2	2	11.1	24.8	226	3.7	0.00E+00	193,600,000	355,900,000	0.73
	X2C5C9	COX1	Cytochrome *c* oxidase subunit 1	2	2	5.8	41.6	379	3.0	7.89E-04	21,347,000	57,543,000	0.38
	A0A346M047	COX2	Cytochrome *c* oxidase subunit II (fragment)	7	1	46.4	17.0	151	22.8	0.00E+00	1,046,600,000	2,406,000,000	0.38
	H3BNI4	ATP6V0C	V-type proton ATPase proteolipid subunit	1	1	8.9	11.6	112	− 2.0	1.00E+00	11,819,000	33,788,000	0.47
	Q496I0	COX7A2	COX7A2 protein	2	2	27.7	9.4	83	10.2	0.00E+00	223,550,000	687,660,000	0.32

Table 6 (continued)

Pathway	Protein ID	Gene name	Protein name	Peptides	Unique peptides	Sequence coverage [%]	Mol. weight [kDa]	Sequence length	Score	*Q* value	Intensity H	Intensity L	Ratio H/L
	COX6C	COX6C	Cytochrome *c* oxidase subunit 6C	2	2	40.0	8.8	75	5.0	0.00E+00	24,314,000	57,899,000	0.34
	COX41	COX4I1	Cytochrome *c* oxidase subunit 4 isoform 1, mitochondrial	8	8	45.6	19.6	169	28.4	0.00E+00	1,057,000,000	2,524,600,000	0.40
	AT12A	ATP12A	Potassium-transporting ATPase alpha chain 2	6	1	5.3	115.5	1039	− 2.0	1.00E+00	25,608,000	48,153,000	0.50
	ATPG	ATP5F1C	ATP synthase subunit gamma, mitochondrial	11	1	36.8	32.2	291	102.1	0.00E+00	610,730,000	1,752,800,000	0.61
	ATPD	ATP5F1D	ATP synthase subunit delta, mitochondrial	3	3	22.6	17.5	168	22.0	0.00E+00	173,290,000	378,660,000	0.59
	ATP5I	ATP5ME	ATP synthase subunit e, mitochondrial	4	4	42.0	7.9	69	10.4	0.00E+00	139,860,000	416,580,000	0.28
	ATPK	ATP5MF	ATP synthase subunit f, mitochondrial	3	3	39.4	10.9	94	15.6	0.00E+00	146,600,000	369,660,000	0.57
	E9PN17	ATP5MG	ATP synthase subunit g, mitochondrial	3	3	48.7	8.5	76	15.1	0.00E+00	501,810,000	1,039,800,000	0.45
	Q5QNZ2	ATP5PB	ATP synthase F(0) complex subunit B1, mitochondrial	9	9	49.7	22.3	195	323.3	0.00E+00	1,074,900,000	2,486,300,000	0.46
	ATP5H	ATP5PD	ATP synthase subunit d, mitochondrial	8	8	59.0	18.5	161	78.9	0.00E+00	525,070,000	965,510,000	0.39
	ATPO	ATP5PO	ATP synthase subunit O, mitochondrial	8	8	54.5	23.3	213	82.2	0.00E+00	1,495,600,000	3,024,300,000	0.56
	VPP1	ATP6V0A1	V-type proton ATPase 116 kDa subunit a isoform 1	10	9	14.8	95.8	831	51.9	0.00E+00	98,038,000	557,300,000	0.35
	R4GN72	ATP6V0D1	V-type proton ATPase subunit d 1	7	7	25.5	31.7	274	21.2	0.00E+00	258,530,000	806,720,000	0.31
	VATA	ATP6V1A	V-type proton ATPase catalytic subunit A	18	18	41.3	68.3	617	277.6	0.00E+00	1,191,800,000	3,218,800,000	0.37
	VATB2	ATP6V1B2	V-type proton ATPase subunit B, brain isoform	15	15	45.6	56.5	511	127.2	0.00E+00	583,390,000	2,310,600,000	0.35
	A0A024R9I0	ATP6V1C1	V-type proton ATPase subunit C	11	11	27.7	43.9	382	36.3	0.00E+00	105,790,000	524,300,000	0.36
	Q53Y06	ATP6V1E1	ATPase, H+ transporting, lysosomal 31 kDa, V1 subunit E isoform 1	6	6	25.2	26.1	226	38.1	0.00E+00	226,190,000	457,540,000	0.46
	A4D1K0	ATP6V1F	V-type proton ATPase subunit F	3	3	33.6	13.4	119	7.7	0.00E+00	72,747,000	287,010,000	0.62
	A0A024R883	ATP6V1G1	V-type proton ATPase subunit G	3	3	29.7	13.8	118	22.3	0.00E+00	121,660,000	150,890,000	0.58
	A0A024R7X3	ATP6V1H	V-type proton ATPase subunit H	6	6	17.6	54.2	465	26.3	0.00E+00	33,783,000	166,330,000	0.37
	COX15	COX15	Cytochrome *c* oxidase assembly protein COX15 homolog	4	4	11.0	46.0	410	6.5	0.00E+00	52,507,000	160,350,000	0.47
	A0A343FH12	COX3	Cytochrome *c* oxidase subunit 3	2	2	13.4	30.0	261	3.6	0.00E+00	251,800,000	620,670,000	0.40
	H3BNX8	COX5A		3	3	20.3	17.2	153	7.1		489,640,000	1,451,700,000	0.67

Table 6 (continued)

Pathway	Protein ID	Gene name	Protein name	Peptides	Unique peptides	Sequence coverage [%]	Mol. weight [kDa]	Sequence length	Score	*Q* value	Intensity H	Intensity L	Ratio H/L
			Cytochrome *c* oxidase subunit 5A, mitochondrial							0.00E+00			
	COX5B	COX5B	Cytochrome *c* oxidase subunit 5B, mitochondrial	4	4	24.8	13.7	129	9.1	0.00E+00	237,370,000	754,990,000	0.33
	CX6B1	COX6B1	Cytochrome *c* oxidase subunit 6B1	4	4	57.0	10.2	86	32.2	0.00E+00	278,190,000	1,028,600,000	0.28
	CY1	CYC1	Cytochrome c1, heme protein, mitochondrial	8	8	31.1	34.5	315	80.4	0.00E+00	426,190,000	876,770,000	0.51
	Q5T1Z0	LHPP	Phospholysine phosphohistidine inorganic pyrophosphate phosphatase	1	1	14.2	22.9	212	1.8	9.74E-03	0	20,832,000	–
	D8VCQ0	ND4	NADH-ubiquinone oxidoreductase chain 4 (fragment)	1	1	3.8	29.6	266	2.2	3.36E-03	3,604,800	7,493,900	0.44
	Q7Z518	NDUFA10	NADH dehydrogenase [ubiquinone] 1 alpha subcomplex subunit 10, mitochondrial	5	5	18.6	40.7	354	14.3	0.00E+00	46,879,000	194,320,000	0.31
	NDUAD	NDUFA13	NADH dehydrogenase [ubiquinone] 1 alpha subcomplex subunit 13	4	4	33.3	16.7	144	12.4	0.00E+00	43,461,000	261,780,000	0.34
	NDUA2	NDUFA2	NADH dehydrogenase [ubiquinone] 1 alpha subcomplex subunit 2	2	2	31.3	10.9	99	5.9	0.00E+00	35,677,000	165,030,000	0.24
	NDUA4	NDUFA4	Cytochrome *c* oxidase subunit NDUFA4	2	2	27.2	9.4	81	30.4	0.00E+00	99,542,000	1,041,400,000	0.28
	NDUA5	NDUFA5	NADH dehydrogenase [ubiquinone] 1 alpha subcomplex subunit 5	3	3	35.3	13.5	116	20.4	0.00E+00	126,370,000	440,540,000	0.46
	NDUA8	NDUFA8	NADH dehydrogenase [ubiquinone] 1 alpha subcomplex subunit 8	6	6	48.8	20.1	172	15.3	0.00E+00	75,771,000	226,560,000	0.33
	NDUA9	NDUFA9	NADH dehydrogenase [ubiquinone] 1 alpha subcomplex subunit 9, mitochondrial	9	9	30.5	38.4	338	22.1	0.00E+00	38,134,000	212,250,000	0.38
	H3BNK3	NDUFAB1	Acyl carrier protein (fragment)	1	1	12.6	12.1	111	20.7	0.00E+00	91,383,000	220,140,000	0.41
	NDUB1	NDUFB1	NADH dehydrogenase [ubiquinone] 1 beta subcomplex subunit 1	3	3	34.5	7.0	58	5.4	0.00E+00	52,572,000	104,780,000	0.46
	H3BPJ9	NDUFB10	NADH dehydrogenase [ubiquinone] 1 beta subcomplex subunit 10	4	4	31.7	19.3	161	22.9	0.00E+00	68,400,000	353,550,000	0.41
	NDUBB	NDUFB11	NADH dehydrogenase [ubiquinone] 1 beta subcomplex subunit 11, mitochondrial	3	3	33.5	17.9	158	16.2	0.00E+00	40,408,000	192,110,000	0.31
	C9JKQ2	NDUFB3	NADH dehydrogenase [ubiquinone] 1 beta subcomplex subunit 3 (fragment)	2	2	27.7	7.6	65	3.0	7.84E-04	19,660,000	91,217,000	0.33
	NDUB4	NDUFB4	NADH dehydrogenase [ubiquinone] 1 beta subcomplex subunit 4	2	2	21.7	15.2	129	6.3	0.00E+00	15,764,000	129,660,000	0.40
	NDUB8	NDUFB8	NADH dehydrogenase [ubiquinone] 1 beta subcomplex subunit 8, mitochondrial	3	3	22.6	21.8	186	9.8	0.00E+00	38,897,000	134,110,000	0.34
	A0A3B3IT57	NDUFB9		3	3	34.1	17.2	138	13.8		47,909,000	178,250,000	0.26

Table 6 (continued)

Pathway	Protein ID	Gene name	Protein name	Peptides	Unique peptides	Sequence coverage [%]	Mol. weight [kDa]	Sequence length	Score	*Q* value	Intensity H	Intensity L	Ratio H/L
			NADH dehydrogenase [ubiquinone] 1 beta subcomplex subunit 9							0.00E+00			
	E5KRK5	NDUFS1	Mitochondrial NADH-ubiquinone oxidoreductase 75 kDa subunit	18	18	33.4	79.5	727	146.6	0.00E+00	87,635,000	1,424,000,000	0.27
	NDUS2	NDUFS2	NADH dehydrogenase [ubiquinone] iron-sulfur protein 2, mitochondrial	9	9	26.6	46.4	406	23.2	0.00E+00	255,210,000	555,800,000	0.40
	NDUS3	NDUFS3	NADH dehydrogenase [ubiquinone] iron-sulfur protein 3, mitochondrial	8	8	39.4	30.2	264	62.5	0.00E+00	303,550,000	1,007,100,000	0.38
	H0Y9M8	NDUFS4	NADH dehydrogenase [ubiquinone] iron-sulfur protein 4, mitochondrial (fragment)	1	1	12.9	13.5	116	4.1	0.00E+00	22,776,000	124,620,000	0.20
	Q6IBA0	NDUFS5	NADH dehydrogenase (ubiquinone) Fe-S protein 5, 15 kDa (NADH-coenzyme Q reductase)	5	5	45.3	12.5	106	6.0	0.00E+00	13,539,000	83,631,000	0.36
	B7Z4P1	NDUFS7	cDNA FLJ58024, highly similar to NADH-ubiquinone oxidoreductase 20 kDa subunit, mitochondrial	1	1	6.1	15.8	148	2.2	3.38E-03	89,666,000	146,530,000	1.06
	E9PKH6	NDUFS8	NADH dehydrogenase [ubiquinone] iron-sulfur protein 8, mitochondrial (fragment)	2	2	19.6	15.9	138	6.0	0.00E+00	25,384,000	70,988,000	0.38
	G3V0I5	NDUFV1	NADH dehydrogenase [ubiquinone] flavoprotein 1, mitochondrial	4	4	12.3	50.1	457	9.4	0.00E+00	25,550,000	98,424,000	0.34
	Q9UEH5	NDUFV2	24-kDa subunit of complex I (fragment)	4	4	23.4	25.4	231	16.5	0.00E+00	120,810,000	407,130,000	0.33
	IPYR2	PPA2	Inorganic pyrophosphatase 2, mitochondrial	9	3	38.6	37.9	334	38.4	0.00E+00	815,730,000	1,743,800,000	0.42
	A0A024QZ30	SDHA	Succinate dehydrogenase [ubiquinone] flavoprotein subunit, mitochondrial	20	20	44.9	72.7	664	200.0	0.00E+00	1,096,500,000	2,950,800,000	0.44
	SDHB	SDHB	Succinate dehydrogenase [ubiquinone] iron-sulfur subunit, mitochondrial	6	2	24.3	31.6	280	17.3	0.00E+00	143,030,000	516,360,000	0.37
	D3DVH1	SDHC	Succinate dehydrogenase complex, subunit C, integral membrane protein, 15 kDa, isoform CRAa	3	3	35.2	11.3	105	6.8	0.00E+00	68,060,000	130,150,000	0.46
	A0A024R5E5	TCIRG1	V-type proton ATPase subunit a	8	7	11.8	93.0	830	29.0	0.00E+00	139,450,000	227,300,000	0.73
	QCR9	UQCR10	Cytochrome b-c1 complex subunit 9	2	2	38.1	7.3	63	12.3	0.00E+00	260,330,000	491,890,000	0.52
	QCR7	UQCRB	Cytochrome b-c1 complex subunit 7	4	4	36.0	13.5	111	13.2	0.00E+00	208,330,000	523,300,000	0.37
	QCR1	UQCRC1	Cytochrome b-c1 complex subunit 1, mitochondrial	15	15	45.8	52.6	480	205.2	0.00E+00	1,326,400,000	3,772,100,000	0.43
	QCR2	UQCRC2	Cytochrome b-c1 complex subunit 2, mitochondrial	15	15	43.9	48.4	453	142.7	0.00E+00	1,718,400,000	3,636,100,000	0.43
	A0A384NPX8	UQCRFS1	Cytochrome b-c1 complex subunit Rieske, mitochondrial	4	4	15.3	29.7	274	16.3	0.00E+00	79,904,000	211,540,000	0.34

Table 6 (continued)

Pathway	Protein ID	Gene name	Protein name	Peptides	Unique peptides	Sequence coverage [%]	Mol. weight [kDa]	Sequence length	Score	*Q* value	Intensity H	Intensity L	Ratio H/L
	QCR8	UQCRQ	Cytochrome b-c1 complex subunit 8	2	2	26.7	8.3	75	8.3	0.00E+00	88,536,000	237,890,000	0.57
Lactate shuttle	B4E106	MCT1	cDNA FLJ53399, highly similar to monocarboxylate transporter 1	2	2	6.7	51.9	480	21.3	0.00E+00	23,799,000	115,420,000	0.53
	MOT4	MCT4	Monocarboxylate transporter 4	7	7	16.1	49.469	465	43.453	0.00E+00	818,320,000	2,103,700,000	0.38

– means the protein expressed in the L group but not in the H group. + means the protein expressed in the H group but not in the L group. / means the protein with expressed value 0 in both the H and L groups. Ratio H/L means the ratio of the ivermectin-treated group (SILAC: H) to the no ivermectin-treated group (SILAC: L)

pathway; the upregulated CS, IDH2, and OGDHL in the Kreb's cycle pathway; and the upregulated UQCRH in OXPHOS. PDHB was significantly upregulated in EOC tissues, which catalyzed pyruvate into acetyl-CoA to link glycolysis with the Kreb's cycle. These results clearly demonstrated that EOC relied on both aerobic glycolysis and OXPHOS to produce energy, namely energy metabolism heterogeneity in EOC tissues. The reason why defective complex I was performing a principal role in urinary system oncocytomas and complex III deficiency caused by cytochrome *b* mutations was frequently occurring in thyroid oncocytomas remains to be determined [57]. It suggested that different cancers had totally different pathways. Cancer cells could proceed with high aerobic glycolysis or increased OXPHOS to produce ATP [58]. Even though the "Warburg effect" was very popular, more and more evidence indicated its limitations. The Warburg effect merely emphasized metabolic symbiosis between cancer cells and stroma cells in the microenvironment, with evidence that glycolysis only offered < 50% ATPs for some human cancer cells. Especially, in gynecological cancer cells, such as MCFs and HeLa, OXPHOS had the main position in producing energy [59]. Moreover, OXPHOS and aerobic glycolysis were not always completely independent of one another. To some extent, alterations of the tumor microenvironment (in normoxia and in hypoxia) affected the status of OXPHOS and aerobic glycolysis to produce ATPs [27]. Moreover, a study found that glycolysis inhibitor had an unsatisfactory curative effect, such as drug resistance or strong side effects [60]. On the other hand, recent clinical research found that the mitochondria operated more efficiently in gynecological tumor cells and that those kinds of cancers might be sensitive to OXPHOS inhibitors [61]. Here, some scientists suggested to focus on metabolic target drug, and the real potential method might be combination therapy to block both glycolysis and mitochondrial OXPHOS pathways.

Today, the antiparasite drug ivermectin remains a relatively unknown drug and has been extended to various disease models [62]. Recently, ivermectin has broken through the bondage of traditional clinical medication, and its abilities to inhibit tumor growth in several types of cancers, including ovarian cancer, breast cancer, and colon cancer, have been reported [34]. However, the mechanisms of its anticancer effects remain unclear. IPA-based network analysis of ivermectin (Fig. 6) revealed that ivermectin could regulate the target molecules PKM, OGDHL, ND2, ND5, CYTB, and UQCRH in various ways. For example, ivermectin could regulate PKM, OGDHL, CYTB, ND2, ND5, and UQCRH by influencing the localization of insulin and controlling the expression of cytokine. Additionally, ivermectin could regulate CYTB, ND2, ND5, and PKM by affecting the chemical protein interactions of ABCB1 and ABCG2. Interestingly, PKM as a key enzyme involved in glycolysis could be regulated by

ivermectin through insulin and also could be regulated by ivermectin through downstream target genes of insulin. Also, SILAC quantitative proteomics revealed that the molecular profiling in glycolysis, Kreb's cycle, oxidative phosphorylation, and lactate shuttle pathways was extensively affected by ivermectin (Table 6). The experimental evidence suggested that the molecular mechanisms were complex between ivermectin and energy metabolism pathways. This present study clearly showed that ivermectin suppressed the energy metabolism system by affecting energy metabolism pathways via targeting PFKP, IDH2, IDH3B, ND2, ND5, CYTB, UQCRH, MCT1, and MCT4 (Figs. 9 and 10), and thereby activated apoptosis, promoted cell cycle arrest, and inhibited cell proliferation (Figs. 7 and 8).

In summary, these findings provided novel insights into the energy metabolism pathway changes in EOC and the antitumor effects of ivermectin via targeting energy metabolism pathways in EOC. These altered molecules and their regulators in EOC energy metabolism pathways were the precious resource in the field of ovarian cancer energy metabolism, which offers increasing promise in the in-depth understanding of EOC energy metabolism and the discovery of energy metabolism-based molecular biomarker pattern and novel antitumor targets/drugs to effectively treat EOC in the context of predictive, preventive, and personalized medicine (PPPM) practice.

Strength and limitations

Energy metabolism abnormality is the important pathophysiological characteristics in EOC. This study revealed the changes of key proteins in the Kreb's cycle and oxidative phosphorylation pathways with quantitative mitochondrial proteomics of EOC tissues, the changes of key proteins in the glycolysis pathway with quantitative proteomics of EOC tissues, and the changes of key proteins in lactate shuttle with quantitative proteomics of EOC tissues. These changed key proteins in these energy metabolism pathways were significantly regulated by the drug ivermectin, and ivermectin can inhibit EOC cell proliferation, suppress cell cycle progression, and promote EOC cell apoptosis. These findings, for the first time, provide the complete landscape of molecule profiling

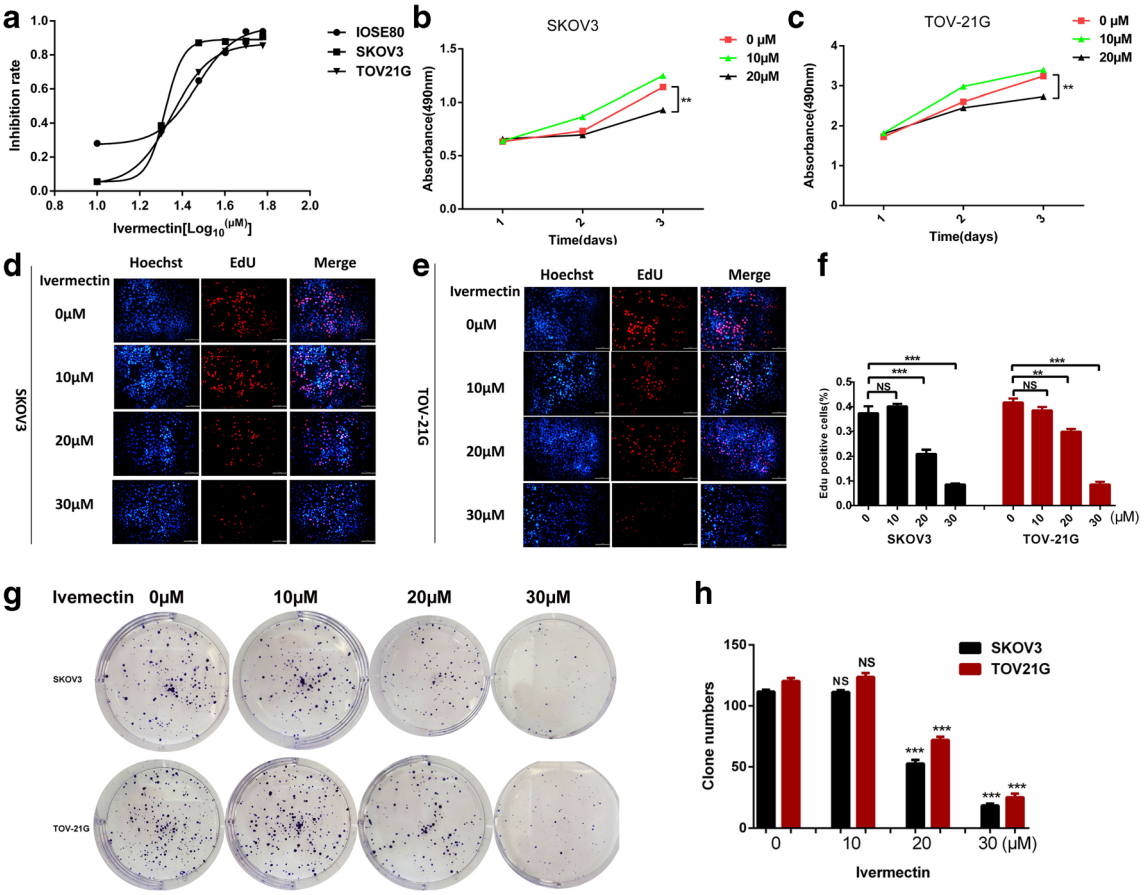

Fig. 7 Ivermectin inhibited ovarian cancer cells proliferation in vitro. **a** Cell viability was measured by the CCK8 assay in IOSE80, SKOV3, and TOV-21G cells treated with the different concentrations of ivermectin for 24 h ($n = 3$, $X = \text{Log}^{(\text{ivermectin concentration})}$). **b** CCK8 cell proliferation test on SKOV3 ($n = 3$). **c** CCK8 cell proliferation test on TOV-21G ($n = 3$). **d** EdU cell proliferation test on SKOV3. **e** EdU cell proliferation test on TOV-21G. **f** Histogram statistics of EdU cell proliferation test on SKOV3 and TOV-21G ($n = 3$). **g** Clonogenic survival test on SKOV3 and TOV-21G. **h** Histogram statistics of clonogenic survival test on SKOV3 and TOV-21G ($n = 3$). $^{*}p < 0.05$, $^{**}p < 0.01$, $^{***}p < 0.001$

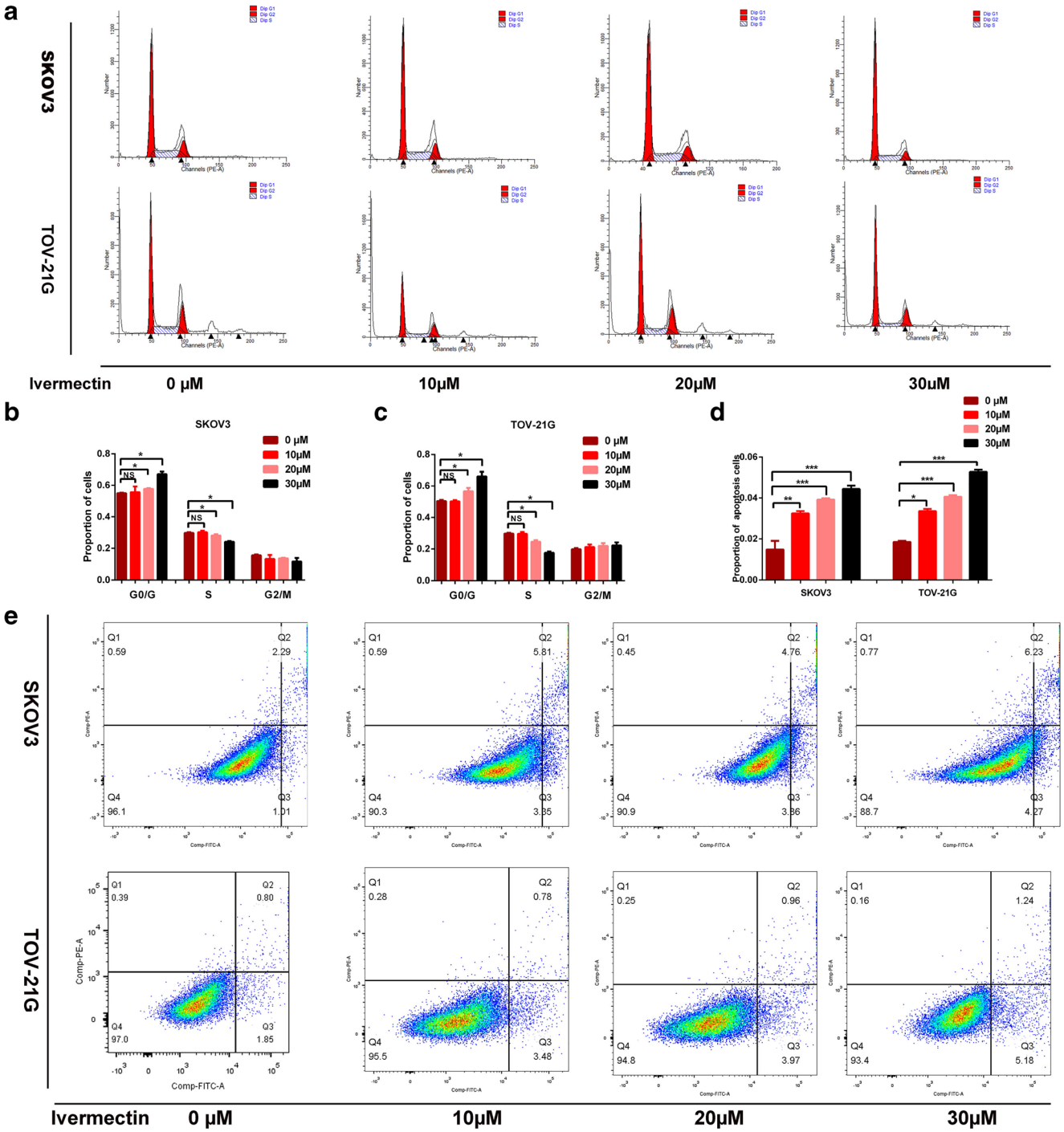

Fig. 8 Ivermectin inhibits cell cycle progression and promotes EOC cell apoptosis. **a** Differences in cell cycle distributions following ivermectin at multiple drug concentrations (0 μM, 10 μM, 20 μM, and 30 μM) by fluorescence-activated cell sorting (FACS). **b** Histogram statistics of cell cycle distributions on SKOV3 ($n = 3$). **c** Histogram statistics of cell cycle distributions on TOV-21G ($n = 3$). **d** Histogram statistics of apoptosis cell percentage on SKOV3 and TOV-21G ($n = 3$). **e** Apoptosis cell percentage following ivermectin at multiple drug concentrations (0 μM, 10 μM, 20 μM, and 30 μM) by fluorescence-activated cell sorting (FACS). $^{*}p < 0.05$, $^{**}p < 0.01$, $^{***}p < 0.001$. EOC, epithelial ovarian carcinoma

changes at the level of protein in the energy metabolism pathways in EOC tissues and their regulation by the drug ivermectin in EOC cell models. These changed molecule profiles in energy metabolism pathways in individualized ovarian cancer patients are the potential biomarker pattern for predictive/prognostic diagnosis, patient stratification, and personalized management of EOC patients, and/or therapeutic targets for effective personalized therapy of EOC patients. Therefore, the main strength of this study is that the landscape of molecule profiling changes at the protein level in energy metabolism

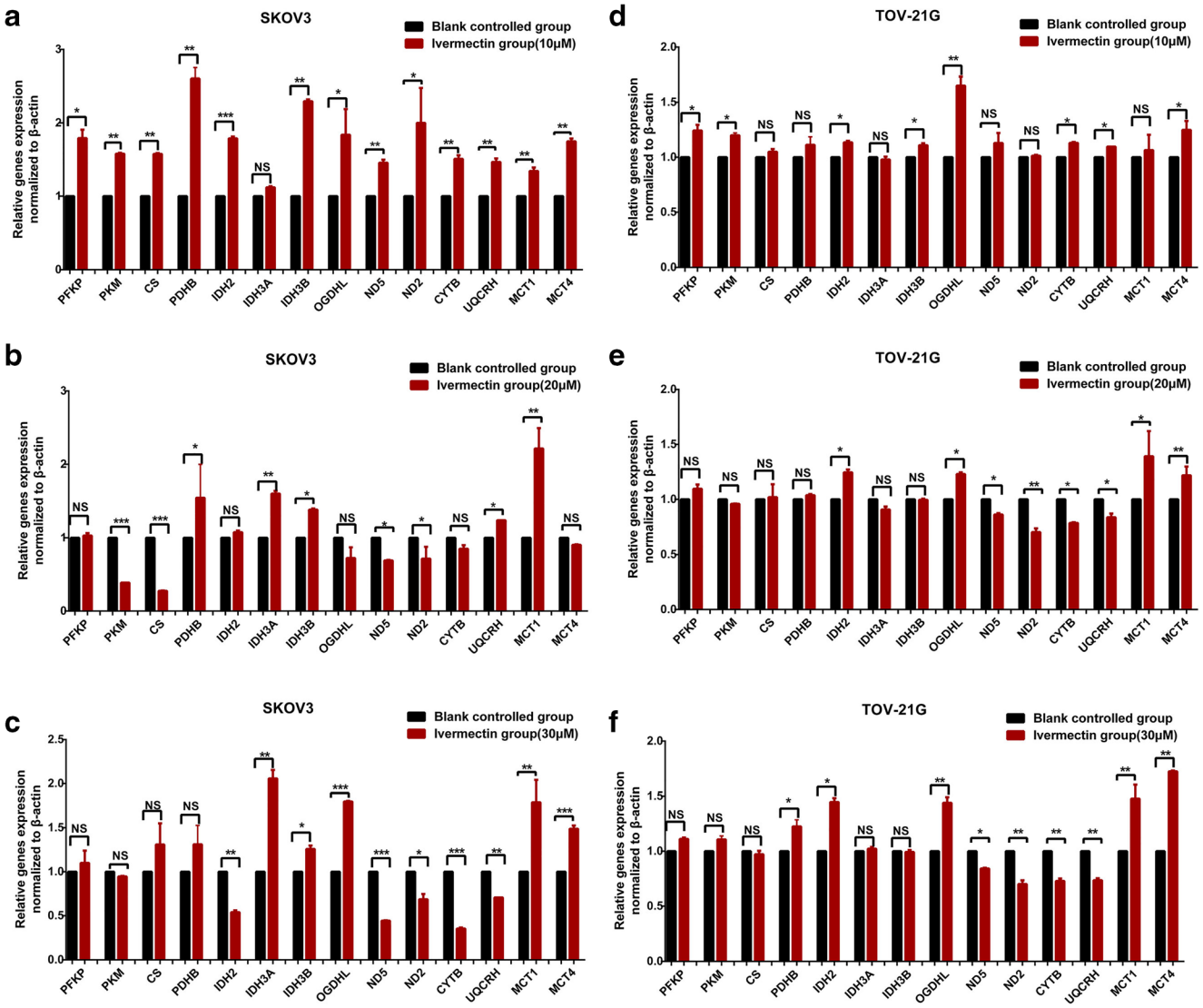

Fig. 9 Ivermectin affects energy metabolism for its anticancer efficiency through targeting PFKP, IDH2, IDH3B, ND2, ND5, CYTB, UQCRH, MCT1, and MCT4 at the mRNA levels analyzed with qPCR. **a**–**f** EOC cells adding ivermectin (10 μM, 20 μM, and 30 μM) and control cell lines (within 0.1% DMSO) were verified by RT-PCR after treatment to identify energy metabolism enzymes and lactate shuttle (MCT1 and MCT2) mRNA expressions ($n = 3$). *$p < 0.05$, **$p < 0.01$, ***$p < 0.001$. PFKP, phosphofructokinase platelet; IDH2, isocitrate dehydrogenase (NADP(+)) 2; IDH3B, isocitrate dehydrogenase (NAD(+)) 3 noncatalytic subunit beta; ND2, mitochondrially encoded NADH dehydrogenase 2; ND5, mitochondrially encoded NADH dehydrogenase 5; UQCRH, ubiquinol-cytochrome *c* reductase hinge protein; MCT1, solute carrier family 16 member 1; MCT4, solute carrier family 16 member 4; EOC, epithelial ovarian carcinoma; CYTB, mitochondrially encoded cytochrome *b*; DMSO, dimethyl sulfoxide; qRT-PCR, quantitative real-time PCR

pathways was revealed with multiple proteomics strategies in EOC tissues, and these changed molecules can be regulated by the drug ivermectin.

However, one must realize that energy metabolism reprogramming is very complex in EOC, and the findings of this study offer important clues to deeply study energy metabolism abnormality in EOC. The following aspects are proposed to further study EOC energy metabolism abnormality: (i) most of the changed molecules in the energy metabolism pathways are the enzymes, and we will further investigate the activity change of those enzymes. (ii) The mitochondria play important roles in EOC energy metabolism, and we will further investigate the functions and activities of the mitochondria in EOC with multiple methods such the sea horse experiment. (iii) We will further investigate the regulatory mechanism system of EOC energy metabolism abnormality, including lncRNAs such as SNHG3 [17, 63], microRNAs such as miRNA-186-5p [17], RNA-binding proteins such as EIF4A3 [17, 63], and drugs such as ivermectin [63] (including the results of this present study). (iv) The changed molecules in the EOC energy metabolism pathways and their regulatory molecules will be the potential biomarker pattern and effective therapeutic targets for the management of EOC patients in the context of PPPM practice.

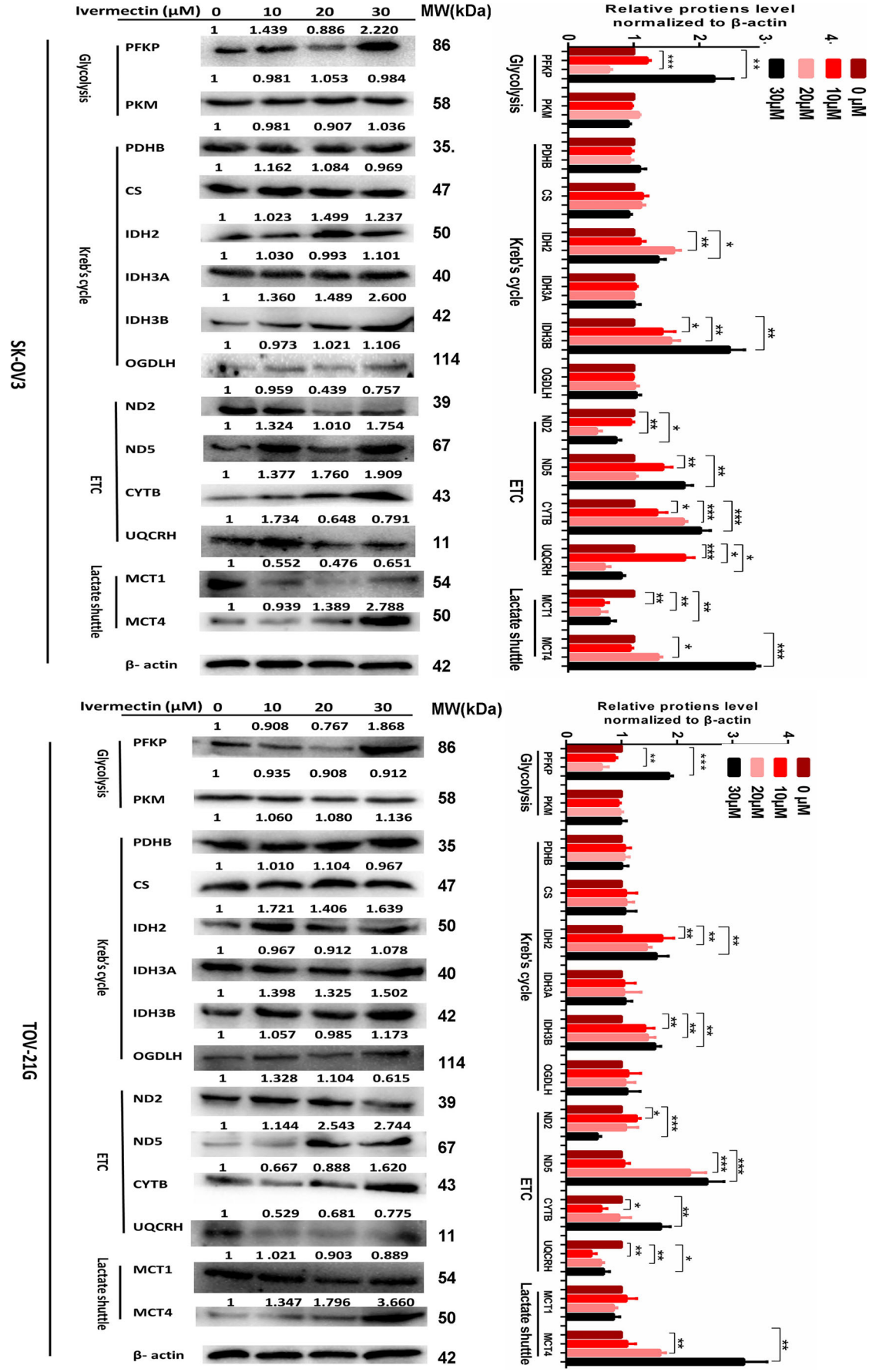
SK-OV3
Ivermectin (μM) 0 10 20 30
MW(kDa)
Glycolysis
PFKP
1 1.439 0.886 2.220
86
PKM
1 0.981 1.053 0.984
58
Kreb's cycle
PDHB
1 0.981 0.907 1.036
35.
CS
1 1.162 1.084 0.969
47
IDH2
1 1.023 1.499 1.237
50
IDH3A
1 1.030 0.993 1.101
40
IDH3B
1 1.360 1.489 2.600
42
OGDLH
1 0.973 1.021 1.106
114
ETC
ND2
1 0.959 0.439 0.757
39
ND5
1 1.324 1.010 1.754
67
CYTB
1 1.377 1.760 1.909
43
UQCRH
1 1.734 0.648 0.791
11
Lactate shuttle
MCT1
1 0.552 0.476 0.651
54
MCT4
1 0.939 1.389 2.788
50
β- actin
42
Relative protiens level normalized to β-actin
0 μM
10μM
20μM
30μM
TOV-21G
Ivermectin (μM) 0 10 20 30
MW(kDa)
Glycolysis
PFKP
1 0.908 0.767 1.868
86
PKM
1 0.935 0.908 0.912
58
Kreb's cycle
PDHB
1 1.060 1.080 1.136
35
CS
1 1.010 1.104 0.967
47
IDH2
1 1.721 1.406 1.639
50
IDH3A
1 0.967 0.912 1.078
40
IDH3B
1 1.398 1.325 1.502
42
OGDLH
1 1.057 0.985 1.173
114
ETC
ND2
1 1.328 1.104 0.615
39
ND5
1 1.144 2.543 2.744
67
CYTB
1 0.667 0.888 1.620
43
UQCRH
1 0.529 0.681 0.775
11
Lactate shuttle
MCT1
1 1.021 0.903 0.889
54
MCT4
1 1.347 1.796 3.660
50
β- actin
42
Relative protiens level normalized to β-actin
0 μM
10μM
20μM
30μM

◀ **Fig. 10** Ivermectin affects energy metabolism for its anticancer efficiency through targeting PFKP, IDH2, IDH3B, ND2, ND5, CYTB, UQCRH, MCT1, and MCT4 at the protein levels analyzed with western blot. EOC cells adding ivermectin (10 μM, 20 μM, and 30 μM) and control cell lines (within 0.1% DMSO) were verified by western blot to detect the protein expression of FPKP, PKM, PDHB,CS, IDH2, IDH3A, IDH3B, OGDHL, ND2, ND5, CYTB, UQCRH, MCT1, and MCT4 (n = 3). *p < 0.05, **p < 0.01, ***p < 0.001. PFK, phosphofructokinase platelet; IDH2, isocitrate dehydrogenase (NADP(+)) 2, IDH3A, mitochondrial isocitrate dehydrogenase [NAD] subunit alpha; IDH3B, isocitrate dehydrogenase (NAD(+)) 3 noncatalytic subunit beta; ND2, mitochondrially encoded NADH dehydrogenase 2; ND5, mitochondrially encoded NADH dehydrogenase 5; UQCRH:, ubiquinol-cytochrome *c* reductase hinge protein; MCT1, solute carrier family 16 member 1; MCT4, solute carrier family 16 member 4; EOC, epithelial ovarian carcinoma; CYTB, mitochondrially encoded cytochrome *b*; DMSO, dimethyl sulfoxide; PKM, pyruvate kinase muscle; PDHB, pyruvate dehydrogenase E1 subunit beta; CS, citrate synthase; OGDHL, oxoglutarate dehydrogenase L

Moreover, one must also note that the SILAC quantification results of ivermectin-treated TOV-21G cells (Table 6) were not fully consistent with PCR and western blot quantification results of ivermectin-treated TOV-21G (Figs. 9 and 10), which might be due to several factors: (i) There are lots of proteoforms with much different abundance that are derived from the same one gene, because of many factors such as alternative RNA splicing and protein PTMs [52, 53, 64]. Protein is the umbrella term for all proteoforms encoded by the same gene [65, 66]. (ii) Each proteoform should have its corresponding specific antibody. The commercially available antibodies used in this study were not the proteoform-specific antibodies. (iii) In the process from gene to proteoforms, there are lots of alternative RNA splicing and PTMs [52, 65, 66], which might result in much difference between the gene and protein (exactly speaking, proteoforms). It can be evidenced by the difference between mRNA and protein expressions of vimentin and multidrug resistance-associated protein 1 (MRP1) in lung squamous carcinoma in our other study [67]. The final abundance of a proteoform is determined by the balance between protein synthesis and degradation system at a given condition. Thus, the abundance of a protein (exactly, proteoform) is dynamically changed with the given conditions. Therefore, in order to accurately reveal the effect of ivermectin on the key molecules in EOC energy metabolism pathways, we propose in future studies to investigate the dose-dependent effect (e.g., 0, 5, 10, 20, 30, 40, and 50 μM ivermectin treatment) and time-dependent effect (e.g., 0, 6, 12, 24, 48, and 72 h after a given ivermectin treatment) of ivermectin on each key molecule in EOC energy metabolism pathways at the levels of mRNA and protein. Anyway, our study clearly demonstrated that ivermectin regulated a wide range of key molecules in energy metabolism pathways—glycolysis, Kreb's cycle, oxidative phosphorylation, and lactate shuttle, which suggests that energy metabolism pathways might be the drug target of ivermectin for its anticancer effects on EOC.

Conclusion and recommendation

Energy metabolism abnormality is the hallmark in EOC. For the first time, this study used iTRAQ quantitative proteomics and mitochondrial proteomics approaches to reveal the changed molecule landscape of energy metabolism pathways in ovarian cancer, with the upregulated key protein molecules PKM2 in glycolysis; IDH2, CS, and OGDHL in Kreb's cycle; UQCRH in oxidative phosphorylation; and MCT1 and MCT4 in lactate shuttle pathways, and SILAC quantitative proteomics, immunoaffinity blot, and RT-qPCR to reveal the antiparasite drug ivermectin effectively inhibited cell proliferation, suppressed cell cycle progression, and promoted cell apoptosis of EOC cells through targeting the key protein molecules PFKP and PKM2 in glycolysis; IDH2 and IDH3B in Kreb's cycle; ND2, ND5, CYTB, and UQCRH in OXPHOS; and MCT1 and MCT4 in lactate shuttle. We concluded that (i) the Warburg and reverse Warburg effects coexisted in human ovarian cancer tissues, with the changed molecular profile of energy metabolism pathways; (ii) ivermectin had the antitumor capability in ovarian cancer cells through targeting energy metabolism pathways; and (iii) those altered key molecules in the energy metabolism pathways are the potential molecular pattern biomarkers for patient individualized stratification, predictive/prognostic diagnosis, and personalized treatment of ovarian cancer patients and are therapeutic targets for personalized therapy of ovarian cancer. Therefore, those findings provide new scientific evidence about the understanding of energy metabolism abnormality of ovarian cancer and the anticancer ability of ivermectin and amplifying its clinical applications.

We recommend to strengthen the study of energy metabolism pathways in ovarian cancer with different omics strategies. Multiomics is the effective approach to study energy metabolism abnormality and reveal the molecular profiling changes in energy metabolism pathways—glycolysis, Kreb's cycle, oxidative phosphorylation, and lactate shuttle, and their regulators including lncRNAs such as SNHG3, microRNAs such as miRNA-186-5p, RNA-binding proteins such as EIF4A3, and drugs such as ivermectin. Energy metabolism pathway network-based molecule pattern biomarkers and therapeutic targets have more important scientific merits in EOC in the context of PPPM practice. We also suggest that it is essential to deeply study the functions and activities of those changed molecules in energy metabolism pathways of ovarian cancers for maximum and precise application of these changed molecules in clinical practice.

We propose the following for further PPPM development and practical application based on those changed energy metabolism pathways in ovarian cancer:

(i) Warburg effect and reverse Warburg effect. This study found the coexistence of the Warburg and reverse

Warburg effects in ovarian cancer tissues with the evidence of four enhanced energy metabolism pathways (upregulations of UQCRH in OXPHOS, IDH2, CS, and OGDHL in Kreb's cycle; PKM2 in glycolysis pathways; and MCT1 and MCT4 in lactate shuttle), which clearly indicated the complexity of energy metabolism in ovarian cancer. Thus, one must have a systematic and comprehensive viewpoint to consider the energy metabolism abnormality of ovarian cancer. Also, one must realize that in ovarian cancer tissue, some cells mainly rely on the Warburg effect—the enhanced glycolysis, and some cells mainly rely on the reverse Warburg effect—the enhanced OXPHOS and Kreb's cycle. The ratio of cells in the states of Warburg effect and of reverse Warburg effect, namely the pattern of the altered molecules in four energy metabolism pathways, can be used as biomarkers for patient stratification, predictive/prognostic assessment, and therapeutic targets of ovarian cancer [68].

(ii) Energy metabolism-based therapeutic targets and drugs. Based on the coexistence of the Warburg and reverse Warburg effects in ovarian cancer tissues and those corresponding changed key molecules in energy pathways, some effective targeted drugs can be designed for ovarian cancer management for targeted prevention and therapy. For example, flavonoids had the anti-Warburg effect through targeting PKM2 in glycolysis pathway, HK2, GLUT1, and HIF-1 to modulate key pathways involved in the Warburg phenotype to cut Gordian knot of cancer cell metabolism [69]. This study found that ivermectin effectively inhibited cell proliferation and cell cycle progression and promoted cell apoptosis in ovarian cancer cells, through molecular networks to target PFKP and PKM2 in glycolysis; IDH2 and IDH3B in Kreb's cycle; ND2, ND5, CYTB, and UQCRH in OXPHOS; and MCT1 and MCT4 in lactate shuttle to inhibit ovarian cancer growth. Therefore, flavonoids and ivermectin might be two types of potential drugs to directly and/or indirectly target energy metabolism pathways for ovarian cancer prevention and therapy. Also, measurement of these key molecule changes of energy metabolism pathways can be used as prognostic assessment for preventive response and therapeutic response and patient stratification [70].

(iii) Crucial roles of multiomics. Multiomics offers the great potential for the identification of the altered molecule profiling in energy metabolism pathways of ovarian cancers [71, 72]. For example, iTRAQ quantitative proteomics of whole tissues effectively identified the molecular change profiling of glycolysis pathway in ovarian cancer (Table 3). The iTRAQ quantitative mitochondrial proteomics effectively identified the molecular change profiling of Kreb's cycle and OXPHOS pathways in ovarian cancers (Tables 4 and 5). Quantitative transcriptomics effectively identified the regulatory mechanism of the changed energy metabolism pathways in ovarian cancer [17]. SILC quantitative proteomics effectively identified the molecular changed profiling of four energy metabolism pathways after drug-treated ovarian cancer cells (Table 6). Therefore, multiomics is a powerful tool to identify changes in the molecular pattern of energy metabolism pathways in the context of PPPM practice in ovarian cancer [71, 73].

(iv) Application of individualized patient profiling. Energy metabolism pathway-based molecular pattern changes in combination with individualized patient profiling [70] will precisely stratify patients for personalized treatment and predictive/prognostic assessment of ovarian cancer patients.

Author contributions N.L. carried out the cell experiments, analyzed the data, prepared the figures and tables, and wrote the manuscript. H.L. collected the samples, prepared the mitochondrial samples, and participated in data analysis and table preparation. Y.W. participated in western blot experiments. L.C. collected tumor tissue samples and performed clinical diagnosis. X.Z. conceived the concept, designed the experiments and manuscript, instructed experiments and data analysis, coordinated and obtained the mitochondrial iTRAQ quantitative proteomic data, supervised the results, wrote and critically revised the manuscript, and was responsible for its financial support and the corresponding works. All authors approved the final manuscript.

Funding The authors acknowledge the financial support from the Shandong First Medical University Talent Introduction Funds (to X.Z.) and the Hunan Provincial Hundred Talent Plan (to X.Z.).

Compliance with ethical standards

Competing interests The authors declare that they have no competing interests.

Consent for publication Not applicable

Ethical approval All the patients were informed about the purposes of the study and, consequently, have signed their "consent of the patient." All investigations conformed to the principles outlined in the Declaration of Helsinki and were performed with permission by the responsible Medical Ethics Committee of Xiangya Hospital, Central South University, China.

Abbreviations 1DGE, one-dimensional gel electrophoresis; 3P medicine, predictive, preventive, and personalized medicine (PPPM); ABCB1, ATP binding cassette subfamily B member 1; Abcb1b, ATP-binding cassette, subfamily B (MDR/TAP), member 1B; ABCG2, ATP-binding cassette subfamily G member 2; ACO1, cytoplasmic aconitate hydratase; ADH5, alcohol dehydrogenase 5 class III chi polypeptide; Akt, AKT serine/threonine kinase 1; APC, APC regulator of WNT signaling pathway; APP, amyloid beta precursor protein; ATP, adenosine triphosphate; ATP5G1, ATP synthase membrane subunit c locus 1; ATP6, ATP synthase F0 subunit 6; ATP6V0C, ATPase H+ transporting V0 subunit c; ATP6V1D, ATPase H+ transporting V1 subunit D; AZD2281, olaparib; BRCA1, BRCA1 DNA repair associated; BRCA2, BRCA2 DNA repair associated; CA-125, cancer antigen 125; CAFs,

cancer-associated fibroblasts; CCK8, Cell Counting Kit-8; CML, chronic myeloid leukemia; CoA, acetyl-coenzyme A; COX1, cytochrome *c* oxidase subunit; COX17, cytochrome *c* oxidase copper chaperone COX17; COX2, cytochrome *c* oxidase subunit II; COX4I1, cytochrome *c* oxidase subunit 4I1; COX4I2, cytochrome *c* oxidase subunit 4I2; COX6C, cytochrome *c* oxidase subunit 6C; COX7A2, cytochrome *c* oxidase subunit 7A2; COX7A2L, cytochrome *c* oxidase subunit 7A2-like; CS, citrate synthase; CYP3A4, cytochrome P450 family 3 subfamily A member 4; CYTB, mitochondrially encoded cytochrome *b*; DMSO, dimethyl sulfoxide; DNA, deoxyribonucleic acid; EdU, 5-ethynyl-2′-deoxyuridine; EIF4A3, eukaryotic translation initiation factor 4A3; ENO1, enolase 1; EOC, epithelial ovarian carcinoma; ERK1/2, mitogen-activated protein kinase 3; ETC, electron transport chain; FACS, fluorescence-activated cell sorting; FADH2, 2,4-dienoyl-CoA reductase; FDA, Food and Drug Administration; FH, fumarate hydratase; G0/G, G0/G cell cycle phase; GAPDH, glyceraldehyde-3-phosphate dehydrogenase; GLRB, glycine receptor beta; GM130, golgin A2; GO, Gene Ontology; GPI, glucose-6-phosphate isomerase; IC50, the half maximal inhibitory concentration; IDH2, isocitrate dehydrogenase (NADP(+)) 2; IDH3A, isocitrate dehydrogenase [NAD] subunit alpha, mitochondrial; IDH3B, isocitrate dehydrogenase (NAD(+)) 3 noncatalytic subunit beta; IPA, Ingenuity Pathway Analysis; iTRAQ, isobaric tags for relative and absolute quantitation; K, lysine; KEGG, Kyoto Encyclopedia of Genes and Genomes; KPNB1, karyopherin subunit beta 1; Kreb's cycle, tricarboxylic acid cycle; LC-MS/MS, liquid chromatography-tandem mass spectrometry; LDHA, lactate dehydrogenase A; LDHB, lactate dehydrogenase B; lncRNA, long noncoding RNAs; MAPK1, mitogen-activated protein kinase 1; MAPK13, mitogen-activated protein kinase 13; MAPK3, mitogen-activated protein kinase 3; MCT1, solute carrier family 16 member 1; MCT4, solute carrier family 16 member 4; MCTs, monocarboxylate transporters; MDH2, malate dehydrogenase 2; miRNA, microRNA; M_r, protein molecular weight; mRNA, messenger RNA; MRP1, multidrug resistance-associated protein 1; MRPL41, mitochondrial ribosomal protein L41; MRPL46, mitochondrial ribosomal protein L41; MRPL49, mitochondrial ribosomal protein L49; MRPL51, mitochondrial ribosomal protein L51; MRPL52, mitochondrial ribosomal protein L52; MRPL53, mitochondrial ribosomal protein L53; MRPL54, mitochondrial ribosomal protein L54; MRPL55, mitochondrial ribosomal protein L55; MRPS10, mitochondrial ribosomal protein S10; MRPS12, mitochondrial ribosomal protein S12; MRPS15, mitochondrial ribosomal protein S15; MRPS17, mitochondrial ribosomal protein S17; MRPS21, mitochondrial ribosomal protein S21; MRPS23, mitochondrial ribosomal protein S23; MRPS33, mitochondrial ribosomal protein S33; MRPS6, mitochondrial ribosomal protein S6; MRPS9, mitochondrial ribosomal protein S9; mtDEPs, mitochondrial differentially expressed proteins; mTOR, mechanistic target of rapamycin kinase; NADH, mitochondrially encoded NADH dehydrogenase 1; ND2, mitochondrially encoded NADH dehydrogenase 2; ND5, mitochondrially encoded NADH dehydrogenase 5; NFKBIA, NFKB inhibitor alpha; OGDHL, oxoglutarate dehydrogenase L; OXPHOS, oxidative phosphorylation; p21, cyclin-dependent kinase inhibitor 1A; p27, cyclin-dependent kinase inhibitor 1B; P2RX4, purinergic receptor P2X 4; P2RX7, purinergic receptor P2X 7; PAK1, p21 (RAC1)-activated kinase 1; PARP, polyADP-ribose polymerase inhibitor; PCK2, phosphoenolpyruvate carboxykinase [GTP], mitochondrial; PDC, pyruvate dehydrogenase complex; PDHB, pyruvate dehydrogenase E1 subunit beta; PFKP, phosphofructokinase, platelet; p*I*, isoelectric point; PKM, pyruvate kinase muscle; PKM2, pyruvate kinase M2; PPPM, predictive, preventive, and personalized medicine; PTMs, posttranslational modifications; QCR6, mitochondrial cytochrome b-c1 complex subunit 6; qRT-PCR, quantitative real-time PCR; R, arginine; Rbp, SURP and G-patch domain containing 1; RNA, ribonucleic acid; ROS, reactive oxygen species; SCX, strong cation exchange chromatography; SD, standard deviation; SDT, N-hydroxysuccinimide; SILAC, stable isotope labeling with amino acids in cell culture; SNHG3, small nucleolar RNA host gene 3; STAT3, signal transducer and activator of transcription 3; SUCLG2, succinate–CoA ligase GDP-forming subunit beta; TNF, tumor necrosis factor; TOMM20, translocase of outer mitochondrial membrane 20; UQCRH, ubiquinol-cytochrome *c* reductase hinge protein; VDAC1, voltage-dependent anion channel 1

References

1. Chan JK, Cheung MK, Husain A, Teng NN, West D, Whittemore AS, et al. Patterns and progress in ovarian cancer over 14 years. Obstet Gynecol. 2006;108:521–8. https://doi.org/10.1097/01.AOG.0000231680.58221.a7.
2. Siegel RL, Miller KD, Jemal A. Cancer statistics, 2016. CA Cancer J Clin. 2016;66:7–30. https://doi.org/10.3322/caac.21332.
3. Gadducci A, Cosio S, Zola P, Landoni F, Maggino T, Sartori E. Surveillance procedures for patients treated for epithelial ovarian cancer: a review of the literature. Int J Gynecol Cancer. 2007;17:21–31. https://doi.org/10.1111/j.1525-1438.2007.00826.x.
4. Smith RA, Manassaram-Baptiste D, Brooks D, Doroshenk M, Fedewa S, Saslow D, et al. Cancer screening in the United States, 2015: a review of current American Cancer Society guidelines and current issues in cancer screening. CA Cancer J Clin. 2015;65:30–54. https://doi.org/10.3322/caac.21261.
5. Buchtel KM, Vogel Postula KJ, Weiss S, Williams C, Pineda M, Weissman SM. FDA approval of PARP inhibitors and the impact on genetic counseling and genetic testing practices. J Genet Couns. 2018;27(1):131–9. https://doi.org/10.1007/s10897-017-0130-7.
6. Lord CJ, Ashworth A. PARP inhibitors: synthetic lethality in the clinic. Science. 2017;355:1152–8. https://doi.org/10.1126/science.aam7344.
7. Jacob F, Meier M, Caduff R, Goldstein D, Pochechueva T, Hacker N, et al. No benefit from combining HE4 and CA125 as ovarian tumor markers in a clinical setting. Gynecol Oncol. 2011;121:487–91. https://doi.org/10.1016/j.ygyno.2011.02.022.
8. Vanni S. Omics of prion diseases. Prog Mol Biol Transl Sci. 2017;150:409–31. https://doi.org/10.1016/bs.pmbts.2017.05.004.
9. Zhan X, Wang X, Long Y, Desiderio DM. Heterogeneity analysis of the proteomes in clinically nonfunctional pituitary adenomas. BMC Med Genet. 2014;7:69. https://doi.org/10.1186/s12920-014-0069-6.
10. Sala S, Van Troys M, Medves S, Catillon M, Timmerman E, Staes A, et al. Expanding the interactome of TES by exploiting TES modules with different subcellular localizations. J Proteome Res. 2017;16:2054–71. https://doi.org/10.1021/acs.jproteome.7b00034.
11. Sassano ML, van Vliet AR, Agostinis P. Mitochondria-associated membranes as networking platforms and regulators of cancer cell fate. Front Oncol. 2017;7:174. https://doi.org/10.3389/fonc.2017.00174.
12. Strickertsson JAB, Desler C, Rasmussen LJ. Bacterial infection increases risk of carcinogenesis by targeting mitochondria. Semin Cancer Biol. 2017;47:95–100. https://doi.org/10.1016/j.semcancer.2017.07.003.
13. Wang Y, Zhang J, Li B, He QY. Proteomic analysis of mitochondria: biological and clinical progresses in cancer. Expert Rev Proteomics. 2017;14:891–903. https://doi.org/10.1080/14789450.2017.1374180.
14. Mintz HA, Yawn DH, Safer B, Bresnick E, Liebelt AG, Blailock ZR, et al. Morphological and biochemical studies of isolated mitochondria from fetal, neonatal, and adult liver and from neoplastic tissues. J Cell Biol. 1967;34:513–23.
15. Chen M, Huang H, He H, Ying W, Liu X, Dai Z, et al. Quantitative proteomic analysis of mitochondria from human ovarian cancer cells and their paclitaxel-resistant sublines. Cancer Sci. 2015;106:1075–83. https://doi.org/10.1111/cas.12710.

16. Li N, Li H, Cao L, Zhan X. Quantitative analysis of the mitochondrial proteome in human ovarian carcinomas. Endocr Relat Cancer. 2018;25:909–31. https://doi.org/10.1530/erc-18-0243.
17. Li N, Zhan X, Zhan X. The lncRNA SNHG3 regulates energy metabolism of ovarian cancer by an analysis of mitochondrial proteomes. Gynecol Oncol. 2018;150:343–54. https://doi.org/10.1016/j.ygyno.2018.06.013.
18. Vyas S, Zaganjor E, Haigis MC. Mitochondria and cancer. Cell. 2016;166:555–66. https://doi.org/10.1016/j.cell.2016.07.002.
19. Li N, Zhan X. Signaling pathway network alterations in human ovarian cancers identified with quantitative mitochondrial proteomics. EPMA J. 2019;10:153–72. https://doi.org/10.1007/s13167-019-00170-5.
20. Kim A. Mitochondria in cancer energy metabolism: culprits or bystanders? Toxicol Res. 2015;31:323–30. https://doi.org/10.5487/tr.2015.31.4.323.
21. Warburg O. On the origin of cancer cells. Science. 1956;123:309–14.
22. Christofk HR, Vander Heiden MG, Harris MH, Ramanathan A, Gerszten RE, Wei R, et al. The M2 splice isoform of pyruvate kinase is important for cancer metabolism and tumour growth. Nature. 2008;452:230–3. https://doi.org/10.1038/nature06734.
23. Birsoy K, Wang T, Chen WW, Freinkman E, Abu-Remaileh M, Sabatini DM. An essential role of the mitochondrial electron transport chain in cell proliferation is to enable aspartate synthesis. Cell. 2015;162:540–51. https://doi.org/10.1016/j.cell.2015.07.016.
24. Pavlides S, Whitaker-Menezes D, Castello-Cros R, Flomenberg N, Witkiewicz AK, Frank PG, et al. The reverse Warburg effect: aerobic glycolysis in cancer associated fibroblasts and the tumor stroma. Cell Cycle. 2009;8:3984–4001. https://doi.org/10.4161/cc.8.23.10238.
25. Bar-Or D, Carrick M, Tanner A 2nd, Lieser MJ, Rael LT, Brody E. Overcoming the Warburg effect: is it the key to survival in sepsis? J Crit Care. 2018;43:197–201. https://doi.org/10.1016/j.jcrc.2017.09.012.
26. Whitaker-Menezes D, Martinez-Outschoorn UE, Lin Z, Ertel A, Flomenberg N, Witkiewicz AK, et al. Evidence for a stroma-epithelial "lactate shuttle" in human tumors: MCT4 is a marker of oxidative stress in cancer-associated fibroblasts. Cell Cycle. 2011;10:1772–83. https://doi.org/10.4161/cc.10.11.15659.
27. Xu XD, Shao SX, Jiang HP, Cao YW, Wang YH, Yang XC, et al. Warburg effect or reverse Warburg effect? A review of cancer metabolism. Oncol Res Treat. 2015;38:117–22. https://doi.org/10.1159/000375435.
28. Chao TK, Huang TS, Liao YP, Huang RL, Su PH, Shen HY, et al. Pyruvate kinase M2 is a poor prognostic marker of and a therapeutic target in ovarian cancer. PLoS One. 2017;12:e0182166. https://doi.org/10.1371/journal.pone.0182166.
29. Suh DH, Kim HS, Kim B, Song YS. Metabolic orchestration between cancer cells and tumor microenvironment as a co-evolutionary source of chemoresistance in ovarian cancer: a therapeutic implication. Biochem Pharmacol. 2014;92:43–54. https://doi.org/10.1016/j.bcp.2014.08.011.
30. Chosidow O, Bernigaud C, Do-Pham G. High-dose ivermectin in malaria and other parasitic diseases: a new step in the development of a neglected drug. Parasite. 2018;25:33. https://doi.org/10.1051/parasite/2018039.
31. Omura S. A splendid gift from the earth: the origins and impact of the Avermectins (Nobel lecture). Angew Chem Int Ed Eng. 2016;55:10190–209. https://doi.org/10.1002/anie.201602164.
32. Crump A. Ivermectin: enigmatic multifaceted 'wonder' drug continues to surprise and exceed expectations. J Antibiot (Tokyo). 2017;70:495–505. https://doi.org/10.1038/ja.2017.11.
33. Drinyaev VA, Mosin VA, Kruglyak EB, Novik TS, Sterlina TS, Ermakova NV, et al. Antitumor effect of avermectins. Eur J Pharmacol. 2004;501:19–23. https://doi.org/10.1016/j.ejphar.2004.08.009.
34. Dou Q, Chen HN, Wang K, Yuan K, Lei Y, Li K, et al. Ivermectin induces cytostatic autophagy by blocking the PAK1/Akt axis in breast cancer. Cancer Res. 2016;76:4457–69. https://doi.org/10.1158/0008-5472.can-15-2887.
35. Zhu M, Li Y, Zhou Z. Antibiotic ivermectin preferentially targets renal cancer through inducing mitochondrial dysfunction and oxidative damage. Biochem Biophys Res Commun. 2017;492:373–8. https://doi.org/10.1016/j.bbrc.2017.08.097.
36. Wang J, Xu Y, Wan H, Hu J. Antibiotic ivermectin selectively induces apoptosis in chronic myeloid leukemia through inducing mitochondrial dysfunction and oxidative stress. Biochem Biophys Res Commun. 2018;497:241–7. https://doi.org/10.1016/j.bbrc.2018.02.063.
37. Kodama M, Kodama T. In vivo loss-of-function screens identify KPNB1 as a new druggable oncogene in epithelial ovarian cancer. Proc Natl Acad Sci U S A. 2017;114:E7301–e7310. https://doi.org/10.1073/pnas.1705441114.
38. Wang LN, Tong SW, Hu HD, Ye F, Li SL, Ren H, et al. Quantitative proteome analysis of ovarian cancer tissues using a iTRAQ approach. J Cell Biochem. 2012;113:3762–72. https://doi.org/10.1002/jcb.24250.
39. Lokich E, Singh RK, Han A, Romano N, Yano N, Kim K, et al. HE4 expression is associated with hormonal elements and mediated by importin-dependent nuclear translocation. Sci Rep. 2014;4:5500. https://doi.org/10.1038/srep05500.
40. Hashimoto H, Messerli SM, Sudo T, Maruta H. Ivermectin inactivates the kinase PAK1 and blocks the PAK1-dependent growth of human ovarian cancer and NF2 tumor cell lines. Drug Discov Ther. 2009;3:243–6.
41. Bartolak-Suki E, Imsirovic J, Nishibori Y, Krishnan R, Suki B. Regulation of mitochondrial structure and dynamics by the cytoskeleton and mechanical factors. Int J Mol Sci. 2017;18. https://doi.org/10.3390/ijms18081812.
42. Schrader M, Costello J, Godinho LF, Islinger M. Peroxisome-mitochondria interplay and disease. J Inherit Metab Dis. 2015;38(4):681–702. https://doi.org/10.1007/s10545-015-9819-7.
43. Rezaul K, Wu L, Mayya V, Hwang SI, Han D. A systematic characterization of mitochondrial proteome from human T leukemia cells. Mol Cell Proteomics. 2005;4:169–81. https://doi.org/10.1074/mcp.M400115-MCP200.
44. Bragoszewski P, Wasilewski M, Sakowska P, Gornicka A, Bottinger L, Qiu J, et al. Retro-translocation of mitochondrial intermembrane space proteins. Proc Natl Acad Sci U S A. 2015;112:7713–8. https://doi.org/10.1073/pnas.1504615112.
45. Johnston IG, Williams BP. Evolutionary inference across eukaryotes identifies specific pressures favoring mitochondrial gene retention. Cell Syst. 2016;2:101–11. https://doi.org/10.1016/j.cels.2016.01.013.
46. Tekade RK, Sun X. The Warburg effect and glucose-derived cancer theranostics. Drug Discov Today. 2017;22:1637–53. https://doi.org/10.1016/j.drudis.2017.08.003.
47. Watanabe H, Takehana K, Date M, Shinozaki T, Raz A. Tumor cell autocrine motility factor is the neuroleukin/phosphohexose isomerase polypeptide. Cancer Res. 1996;56:2960–3.
48. Pavlides S, Vera I, Gandara R, Sneddon S, Pestell RG, Mercier I, et al. Warburg meets autophagy: cancer-associated fibroblasts accelerate tumor growth and metastasis via oxidative stress, mitophagy, and aerobic glycolysis. Antioxid Redox Signal. 2012;16:1264–84. https://doi.org/10.1089/ars.2011.4243.
49. Sullivan LB, Chandel NS. Mitochondrial reactive oxygen species and cancer. Cancer Metab. 2014;2:17. https://doi.org/10.1186/2049-3002-2-17.
50. Sakhuja S, Yun H, Pisu M, Akinyemiju T. Availability of healthcare resources and epithelial ovarian cancer stage of

diagnosis and mortality among Blacks and Whites. J Ovarian Res. 2017;10:57. https://doi.org/10.1186/s13048-017-0352-1.
51. Min HY, Lee HY. Oncogene-driven metabolic alterations in cancer. Biomol Ther (Seoul). 2018;26:45–56. https://doi.org/10.4062/biomolther.2017.211.
52. Zhan X, Long Y, Lu M. Exploration of variations in proteome and metabolome for predictive diagnostics and personalized treatment algorithms: innovative approach and examples for potential clinical application. J Proteome. 2018;188:30–40. https://doi.org/10.1016/j.jprot.2017.08.020.
53. Qian S, Yang Y, Li N, Cheng T, Wang X, Liu J, et al. Prolactin variants in human pituitaries and pituitary adenomas identified with two-dimensional gel electrophoresis and mass spectrometry. Front Endocrinol (Lausanne). 2018;9:468. https://doi.org/10.3389/fendo.2018.00468.
54. Kobierzycki C, Piotrowska A, Latkowski K, Zabel M, Nowak-Markwitz E, Spaczynski M, et al. Correlation of pyruvate kinase M2 expression with clinicopathological data in ovarian cancer. Anticancer Res. 2018;38:295–300. https://doi.org/10.21873/anticanres.12221.
55. DeHart DN, Lemasters JJ, Maldonado EN. Erastin-like anti-Warburg agents prevent mitochondrial depolarization induced by free tubulin and decrease lactate formation in cancer cells. SLAS Discov. 2018;23:23–33. https://doi.org/10.1177/2472555217731556.
56. Yoshida GJ. Metabolic reprogramming: the emerging concept and associated therapeutic strategies. J Exp Clin Cancer Res. 2015;34:111. https://doi.org/10.1186/s13046-015-0221-y.
57. Godinot C, de Laplanche E, Hervouet E, Simonnet H. Actuality of Warburg's views in our understanding of renal cancer metabolism. J Bioenerg Biomembr. 2007;39:235–41. https://doi.org/10.1007/s10863-007-9088-8.
58. Lee M, Yoon JH. Metabolic interplay between glycolysis and mitochondrial oxidation: the reverse Warburg effect and its therapeutic implication. World J Biol Chem. 2015;6:148–61. https://doi.org/10.4331/wjbc.v6.i3.148.
59. Hernandez-Resendiz I, Roman-Rosales A, Garcia-Villa E, Lopez-Macay A, Pineda E, Saavedra E, et al. Dual regulation of energy metabolism by p53 in human cervix and breast cancer cells. Biochim Biophys Acta. 1853;2015:3266–78. https://doi.org/10.1016/j.bbamcr.2015.09.033.
60. Suganuma K, Miwa H, Imai N, Shikami M, Gotou M, Goto M, et al. Energy metabolism of leukemia cells: glycolysis versus oxidative phosphorylation. Leuk Lymphoma. 2010;51:2112–9. https://doi.org/10.3109/10428194.2010.512966.
61. Klepinin A, Ounpuu L, Guzun R, Chekulayev V, Timohhina N, Tepp K, et al. Simple oxygraphic analysis for the presence of adenylate kinase 1 and 2 in normal and tumor cells. J Bioenerg Biomembr. 2016;48:531–48.
62. Jin L, Feng X, Rong H, Pan Z, Inaba Y, Qiu L, et al. The antiparasitic drug ivermectin is a novel FXR ligand that regulates metabolism. Nat Commun. 2013;4:1937. https://doi.org/10.1038/ncomms2924.
63. Li N, Zhan X. Anti-parasite drug ivermectin can suppress ovarian cancer by regulating lncRNA-EIF4A3-mRNA axes. EPMA J. 2020;11:289–309. https://doi.org/10.1007/s13167-020-00209-y.
64. Zhan X, Giorgianni F, Desiderio DM. Proteomics analysis of growth hormone isoforms in the human pituitary. Proteomics. 2005;5:1228–41. https://doi.org/10.1002/pmic.200400987.
65. Zhan X, Li B, Zhan X, Schlüter H, Jungblut PR, Coorssen JR. Innovating the concept and practice of two-dimensional gel electrophoresis in the analysis of proteomes at the proteoform level. Proteomes. 2019;7(4):36. https://doi.org/10.3390/proteomes7040036.
66. Zhan X, Li N, Zhan X, Qian S. Revival of 2DE-LC/MS in proteomics and its potential for large-scale study of human proteoforms. Med One. 2018;3:e180008. https://doi.org/10.20900/mo.20180008.
67. Lu M. Wei Chen, Zhuang W, Zhan X. Label-free quantitative identification of abnormally ubiquitinated proteins as useful biomarkers for human lung squamous cell carcinomas. EPMA J. 2020;11(1):73–94. https://doi.org/10.1007/s13167-019-00197-8.
68. Janssens JP, Schuster K, Voss A. Preventive, predictive, and personalized medicine for effective and affordable cancer care. EPMA J. 2018;9(2):113–23. https://doi.org/10.1007/s13167-018-0130-1.
69. Samec M, Liskova A, Koklesova L, Samuel SM, Zhai K, Buhrmann C, et al. Flavonoids against the Warburg phenotype-concepts of predictive, preventive and personalised medicine to cut the Gordian knot of cancer cell metabolism. EPMA J. 2020;11(3):377–98. https://doi.org/10.1007/s13167-020-00217-y.
70. Golubnitschaja O, Flammer J. Individualised patient profile: clinical utility of Flammer syndrome phenotype and general lessons for predictive, preventive and personalised medicine. EPMA J. 2018;9(1):15–20. https://doi.org/10.1007/s13167-018-0127-9.
71. Lu M, Zhan X. The crucial role of multiomic approach in cancer research and clinically relevant outcomes. EPMA J. 2018;9(1):77–102. https://doi.org/10.1007/s13167-018-0128-8.
72. Li N, Zhan X. Identification of clinical trait-related lncRNA and mRNA biomarkers with weighted gene co-expression network analysis as useful tool for personalized medicine in ovarian cancer. EPMA J. 2019;10(3):273–90. https://doi.org/10.1007/s13167-019-00175-0.
73. Cheng T, Zhan X. Pattern recognition for predictive, preventive, and personalized medicine in cancer. EPMA J. 2017;8(1):51–60. https://doi.org/10.1007/s13167-017-0083-9.

Abbreviations for all particular genes and proteins can be found at the following link: https://www.ncbi.nlm.nih.gov/gene/.

Affiliations

Na Li[1,2,3] · Huanni Li[4] · Ya Wang[2,3] · Lanqin Cao[4] · Xianquan Zhan[1,2,3,5,6]

[1] University Creative Research Initiatives Center, Shandong First Medical University, 6699 Qingdao Road, Jinan 250117, Shandong, People's Republic of China

[2] Key Laboratory of Cancer Proteomics of Chinese Ministry of Health, Xiangya Hospital, Central South University, 87 Xiangya Road, Changsha 410008, Hunan, People's Republic of China

[3] State Local Joint Engineering Laboratory for Anticancer Drugs, Xiangya Hospital, Central South University, 87 Xiangya Road, Changsha 410008, Hunan, People's Republic of China

[4] Department of Obstetrics and Gynecology, Xiangya Hospital, Central South University, 87 Xiangya Road, Changsha 410008, Hunan, People's Republic of China

[5] National Clinical Research Center for Geriatric Disorders, Xiangya Hospital, Central South University, 87 Xiangya Road, Changsha 410008, Hunan, People's Republic of China

[6] Department of Oncology, Xiangya Hospital, Central South University, 87 Xiangya Road, Changsha 410008, Hunan, People's Republic of China